CALIFORNIA STATE UNIVERSITY, NORTHRIDGE

DIFFERENTIATING ROTOR RESPONSE DUE TO RADIAL RUBBING

A thesis submitted in partial satisfaction of the requirements for the degree of Master of Science in

Engineering

by

Robert Francis Beatty

January 1982

This Thesis of Robert Francis Beatty is approved:

Professor J. Paul

Professor L. Nypan

Professor M. C. Ek, Chairman

California State University, Northridge

TABLE OF CONTENTS

LIST OF FIGURES

NOMENCLATURE

a	Fourier coefficient
F	Frictional force, lbs.
K	Bearing or effective stiffness, lbs./inch
m	Mass center
n	Harmonic number
N	Normal force on rotor, lbs.
r	Eccentricity, inches
R	Shaft center radial displacement relative to the stator, inches
S	Shaft center
t	Time, seconds
Y,Z	Coordinate system fixed to stator
Y_R,Z_R	Coordinate system fixed to rotor
β	Precession angle, radians
ϕ_1	Half rotor rub arc, radians
θ	Contact point angle, radians
ω	Spin speed, radians/second
ω_c	Critical speed, radians/second
Δ	Radial clearance between rotor and stator at rest, inches
δ	Radial clearance between bearing outer race and stator at rest, inches
μ	Coefficient of kinetic friction

ABSTRACT

DIFFERENTIATING ROTOR RESPONSE DUE TO RADIAL RUBBING

by

Robert Francis Beatty

Masters of Science in Engineering

Among the factors leading to destructive instability of rotors in high speed, high performance turbomachinery is excessive rubbing between rotating and stationary parts. Although in many designs this is intentional, such as tight-fitting turbine tip seals, uncontrolled contact can be disastrous.

This thesis proposes a mathematical rationale of rubbing identification, defines the limits between benign contact and the initiation of a destructive instability based on harmonic spectral data, correlates the results with industry experience, published findings and extensive laboratory tests and details the response format of diagnostic data in actual cases. This detection methodology aids in making practical testing decisions based on a reliable indication of the operating condition.

Criteria to infer rubbing related to simple unbalanced response and to differentiate it from bearing deadband effects are advanced from accelerometer data.

I. OBJECTIVE

SUBJECT

Rotating machinery rubbing detection data prior to the creation of a catastrophic problem, or loss of machine efficiency, has received insufficient treatment in the literature. Lacking details of early warning response characteristics is a significant problem for the analyst. In general, the spectral content produced during rotor rubbing has not been adequately evaluated. The study presented concentrates on a rubbing detection methodology and the ability to differentiate it from additional effects.

OBJECT

General detection techniques to determine rotor rubbing are required, particularly in applications where close-coupled instrumentation and constant inspections are impractical, such as rocket engine turbomachinery. In this case, housing transmissibility is relied upon to monitor the rotor motion. Diagnostic techniques must be developed which are general enough for direct transmission and for the compliant path of the housing. Easily identifiable dynamic response characteristics must be quantified to predict and describe the interaction. Knowledge of these characteristics in data evaluation for correlation with the hardware condition has been somewhat limited.

It is the objective of this thesis to analytically predict and experimentally verify the response of a rotor due to radial rubbing prior to the initiation of a catastrophic problem, such as a destructive rotor instability. Typical evaluations of changes in synchronous response, or the presence of subsynchronous oscillations, will be

expanded to explore the generated higher harmonic frequencies of this nonlinearity. The purpose is to provide a reliable rubbing detection methodology as a diagnostic tool in dynamic data evaluation of all rotating machinery with the use of spectral analysis. This methodology should be capable of defining limits between benign contact, excessive wear, and the initiation of a destructive rotor instability.

Bearing clearance, an additional nonlineaity, is inherent in a rotor/mechanical bearing system and the rotor response can be affected if the clearance is significant. The identification criteria should consider this effect and be able to differentiate it from rubbing. Due to the complexity involved in combining nonlinear effects mathematically, the description of the bearing clearance response will be limited to experimental data and the results of other publications.

II. INTRODUCTION

BACKGROUND

In typical high speed rotating machinery, such as jet engines and rocket engine turbomachinery, there are many instances in which rotor rubs occur. Current interest in fuel efficiency is a consideration which drives the machine design toward closer operating clearances to reduce leakage. The desire for the highest possible performance of rotating machinery increases the probability of radial rotor rubs at the common minimum rotor/stator clearance locations of blade tips and seals. The interference etiology can be described by thermal mismatch, rotor unbalance, aerodynamic and seal forces, misalinement, etc.

The interaction of a rotor with its housing can have an important effect on the rotordynamics. Rotor rubs on the housing generate a frictional force which can drive a rotor to divergent vibration amplitudes in which the rotor precesses in a direction opposite to the direction of rotation. This is called a backward precession. Rubbing therefore plays an important role in dynamic stability. Many authors' description of rubbing implies that rubs are always instability drivers. In practice however, this is not the case since rubbing rotors generally operate fairly well although subject to occasional failure.

A description of the forces produced by rubbing and how they can initiate a rotor instability is significant in understanding the problem. Consider an axial cross-section through a vertical rotor at a seal location. Under a rubbing condition the system would appear as shown in Figure 1 with the rotor temporarily deflected from its

equilibrium position in the center of the stator to contact at point A. The circular stator is considered fixed and rigid in space. There is radial clearance Δ between the rotor and stator.

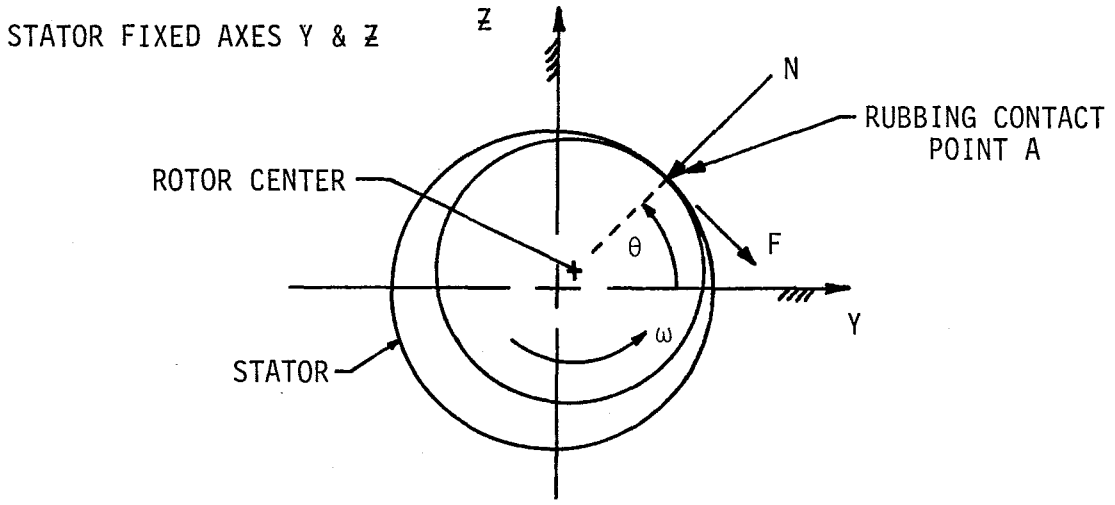

FIGURE 1. AXIAL CROSS-SECTION OF DEFLECTED SYSTEM

The forces on the rotor due to rubbing are the normal force (N) and the frictional force (F):

$$N = K(R - \Delta) \; ; \; R \geq \Delta$$

$$F = \mu N \tag{1}$$

where: Δ = radial clearance between rotor and stator at rest

K = effective stiffness

$R = \sqrt{y^2 + z^2}$

μ = coefficient of kinetic friction

Therefore, the frictional force (F) can be described as componets:

$$F_y = \mu(N)\sin\theta - (N)\cos\theta$$

$$F_z = (N)\sin\theta - \mu(N)\cos\theta \tag{2}$$

$$\sin\theta = \frac{Z}{R} \qquad \cos\theta = \frac{Y}{R} \tag{3}$$

Substituting (1) and (3) into (2):

$$F_y = \mu K(R - \Delta)\frac{Z}{R} - K(R - \Delta)\frac{Y}{R}$$

$$F_Z = -K(R - \Delta)\frac{Z}{R} - \mu K(R - \Delta)\frac{Y}{R} \tag{4}$$

$$F_y = -KY + \mu KZ + \frac{K\Delta}{R}(Y - \mu Z)$$

$$F_Z = -\mu Ky - KZ + \frac{K\Delta}{R}(Z + \mu Y) \tag{5}$$

Writing (5) in matrix form:

$$\begin{Bmatrix} F_y \\ F_Z \end{Bmatrix} = \frac{-K(R - \Delta)}{R}\begin{bmatrix} 1 & -\mu \\ \mu & 1 \end{bmatrix}\begin{Bmatrix} Y \\ Z \end{Bmatrix} \tag{6}$$

Note that this equation is nonlinear. The square stiffness matrix is unsymmetric as shown by the sign of the off-diagonal terms. This unsymmetry indicates that the rotor is potentially unstable as described by Black (1) and Alford(2). Depending on the strength of the tangential friction cross-coupling force, acting opposite to the spin direction, the rotor can go unstable very abruptly in a backward precession in some systems, while in others it may act as a deflection limiter. The deleterious effects of a rotor instability are at a precessional frequency which is less than spin speed, or subsynchronous.

In practice it is difficult to construct a rotor/mechanical bearing system without introducing a built in nonlinearity, that of the bearing "deadband". The bearing outer race to housing clearance is defined as the "deadband" as shown in examples of Figure 2. It is good design practice to operate with the smallest clearance possible,

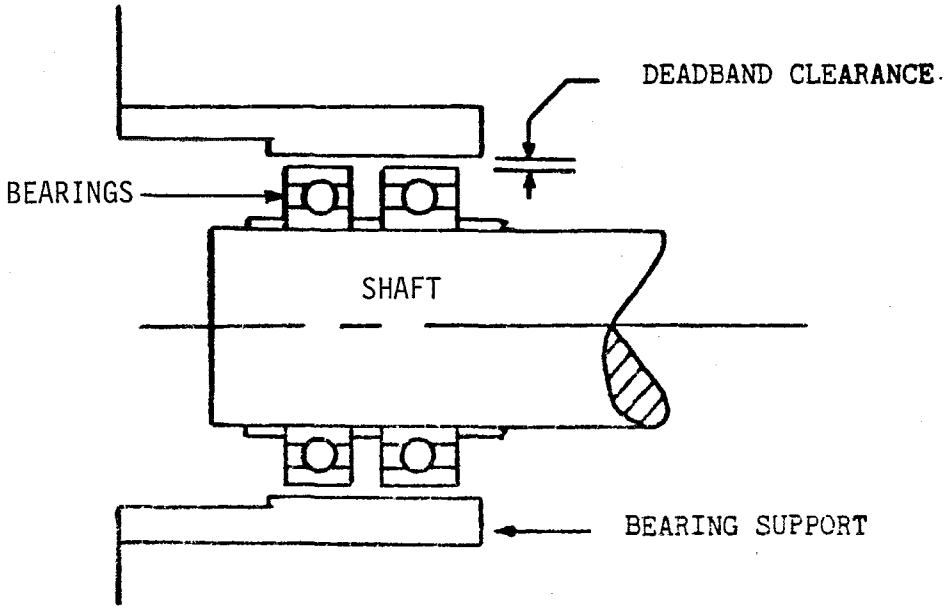

SCHEMATIC REPRESENTATIONS

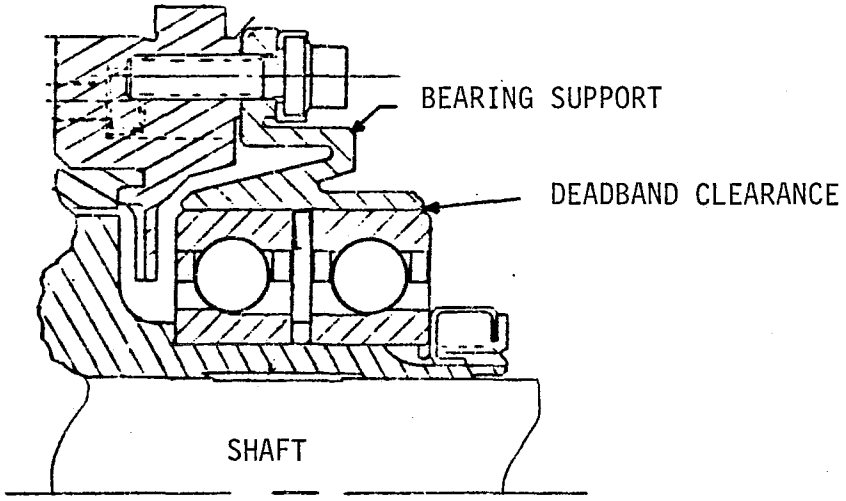

ACTUAL CASE CROSS-SECTION

FIGURE 2. BEARING DEADBAND CLEARANCE DESCRIPTION

preferably tight. However, this clearance is usually present to allow for axial movement of the shaft relative to the housing and dimensional changes due to thermal effects. The radial force deflection curve for motion of the shaft center relative to the fixed stator is shown in Figure 3.

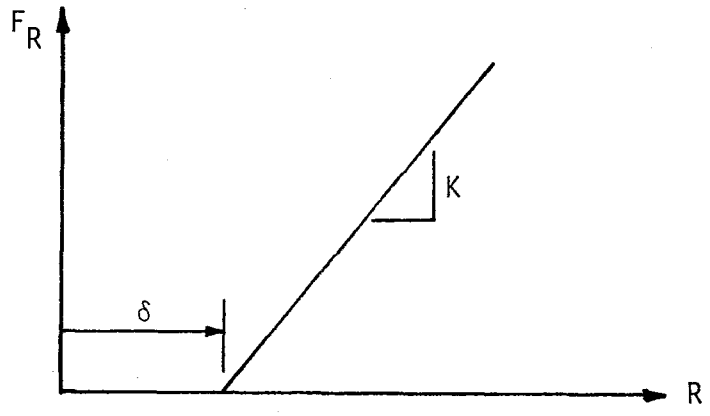

FIGURE 3. RADIAL FORCE DEFLECTION CURVE

F_R = radial force

δ = radial clearance

K = bearing radial stiffness

R = radial displacement of shaft center relative to stator

In this example, the stator is considered to be fixed in space. Also, K is considered constant which is a reasonable approximation for axially preloaded ball bearings. The radial force is:

$$F_R = K(R - \delta) \qquad (7)$$

For $R \geq \delta$

The Y and $\not{z}$ components for $R \geq \delta$ are:

$$F_Y = \frac{-F_R \cdot Y}{R}$$

$$F_{\not{z}} = \frac{-F_R \cdot \not{z}}{R} \tag{8}$$

$$F_Y = -K(R - \delta) \cdot \frac{Y}{R} \tag{9}$$

$$F_{\not{z}} = -K(R - \delta) \cdot \frac{\not{z}}{R}$$

Writing (9) in matrix form:

$$\begin{Bmatrix} F_y \\ F_{\not{z}} \end{Bmatrix} \frac{-K(R - \delta)}{R} \begin{bmatrix} 1 & 0 \\ 0 & 1 \end{bmatrix} \begin{Bmatrix} Y \\ \not{z} \end{Bmatrix} \tag{10}$$

For $R = \sqrt{y^2 + \not{z}^2}$

Again, the force relationships of equation (10) are nonlinear and are similar to those of equation (6) without the frictional effect. The total response will be the sum of these nonlinear effects. Due to the complexities involved in combining these effects using digital or analog computer techniques, the bearing deadband will be assumed to be zero so that the bearing behaves as a linear system. The bearing clearance is mentioned only because its nonlinear effects can alter the predicted rubbing results and experimental data interpretations must keep this under consideration.

LITERATURE

Most rubbing investigators prefer to dwell on the fact that rubbing can cause a backwards precession instability which is detrimental to the machinery and referred to as rotor whirl. Many papers address this aspect, most referencing Den Hartog's (3) explanation of the phenomenon which suggests that as soon as the rotor contacts the stator for any reason, the shaft is set into a violent whirling vibration. Yet, Kascak (4) mentions that many machines are designed with the intention of sustaining rubs occasionally, or systematically, and in some cases, without major secondary damage. As a design policy, this has proven to be difficult and occasionally hazardous.

An example of the detrimental effects of rotor rubbing is shown in Figures 4 and 5. The rubbed surface of an impeller interstage seal from the High Pressure Fuel Turbopump (HPFTP) of the Space Shuttle Main Engine (SSME) is shown in Figure 4. The wear on the mating stator is shown in Figure 5. The increased seal clearance as a result of the illustrated wear can lead to a less violent version of the instability problem described by Ek (5) during the development of this machine.

The literature search can be summarized with a review of a relatively few articles. Ehrich (6) describes rubbing at supercritical operation producing subsynchronous oscillations at the rotor critical speed frequency based upon jet engine experience. Ehrich (7) also observed subsynchronous oscillations at half shaft speed for rotors with excessive bearing clearance. In an additional publication, Ehrich (8) details sum and difference frequencies produced, such as synchronous speed plus the subsynchronous frequency for a rotor with

excessive bearing clearance. He also describes how housing transmissibility can amplify lower frequencies and attenuate high frequencies.

Bently (9) explored rubbing by setting up a special situation on a simple rotor kit. The rotor was operated approximately two and a half to three times the first critical speed. When rubbed, it produced subsynchronous oscillations at fractions of the shaft speed (1/2, 1/3, 1/4, etc.). Bently (10) concluded that rubbing over a portion of a rotor's orbit causes a periodic variation in the effective rotor radial stiffness which can lead to an instability. This he describes in terms of a Mathieu function. In addition, Bently states that partial rubbing due to an off-centered seal can cause half speed backward whirl and produce higher harmonic frequencies at two, three and four times speed. He did not elaborate on these higher harmonic frequencies specifically.

Childs (11) provided a mathematical description of Jeffcott rotor rubbing and the parametric frequencies generated assuming the rub-induced restoring force in terms of a Fourier series expansion. He was able to match Bently's half speed prediction, but was unable to confirm the 1/3 and 1/4 shaft speed frequencies. The possibility of supersynchronous frequency generation was also mentioned, but he also did not elaborate.

In another account, Taylor (12) has reported on the rubbing thermal effects on synchronous unbalance response above and below the rotor critical speed. He showed experimentally that rubbing below the critical speed would set up a detrimental cycle of local heating on the heavy side of the rotor, where the mass center is outside the geometric center. This is followed by shaft distortion, increased

unbalance due to thermal bow, harder rubbing, etc. Above the critical speed no such effect occurs, because the mass center is inside the geometric center and the thermal bow is not accentuated. Thus rubbing on the light side provides heating effects which center the rotor. Figure 6 summarizes this effect in the composite view provided.

The work of these four investigators comprises most of the available literature on rotor rubbing, other than the well documented rubbing instability work. Additional work in this area is warranted with an emphasis on; the early detection of rotor rubbing, the frequencies generated, the severity, and the establishment of a reliable detection method since unnecessary maintenance is undesirable. It is necessary to make the detection analysis applicable for all rotating machinery, not just for rotors operating at many times their lowest critical speed. This knowledge will insure testing can proceed with confidence.

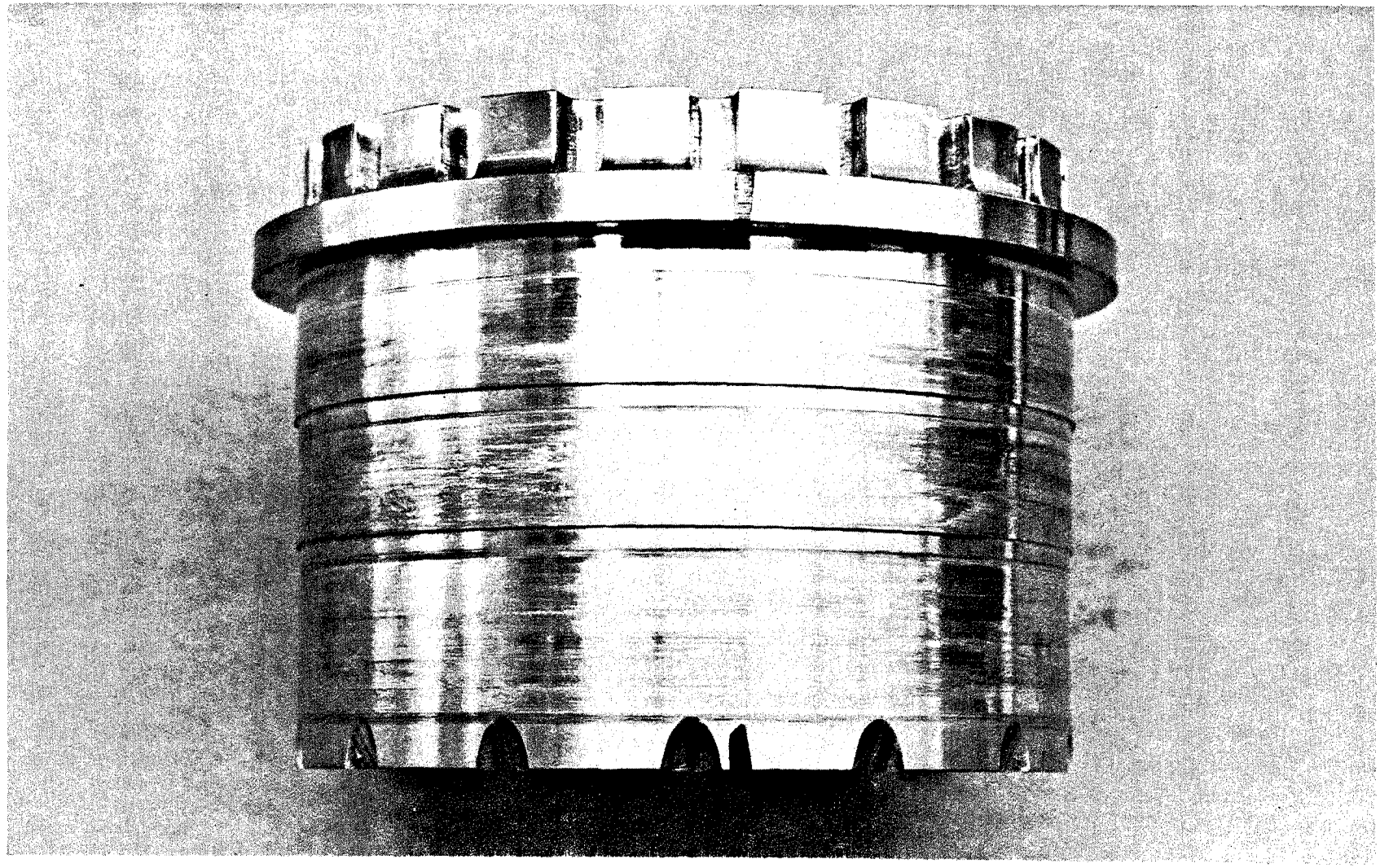

FIGURE 4. SPACE SHUTTLE MAIN ENGINE (SSME) HIGH PRESSURE FUEL TURBOPUMP (HPFTP) 0110R1 RUBBED IMPELLER INTERSTAGE SEAL ROTOR

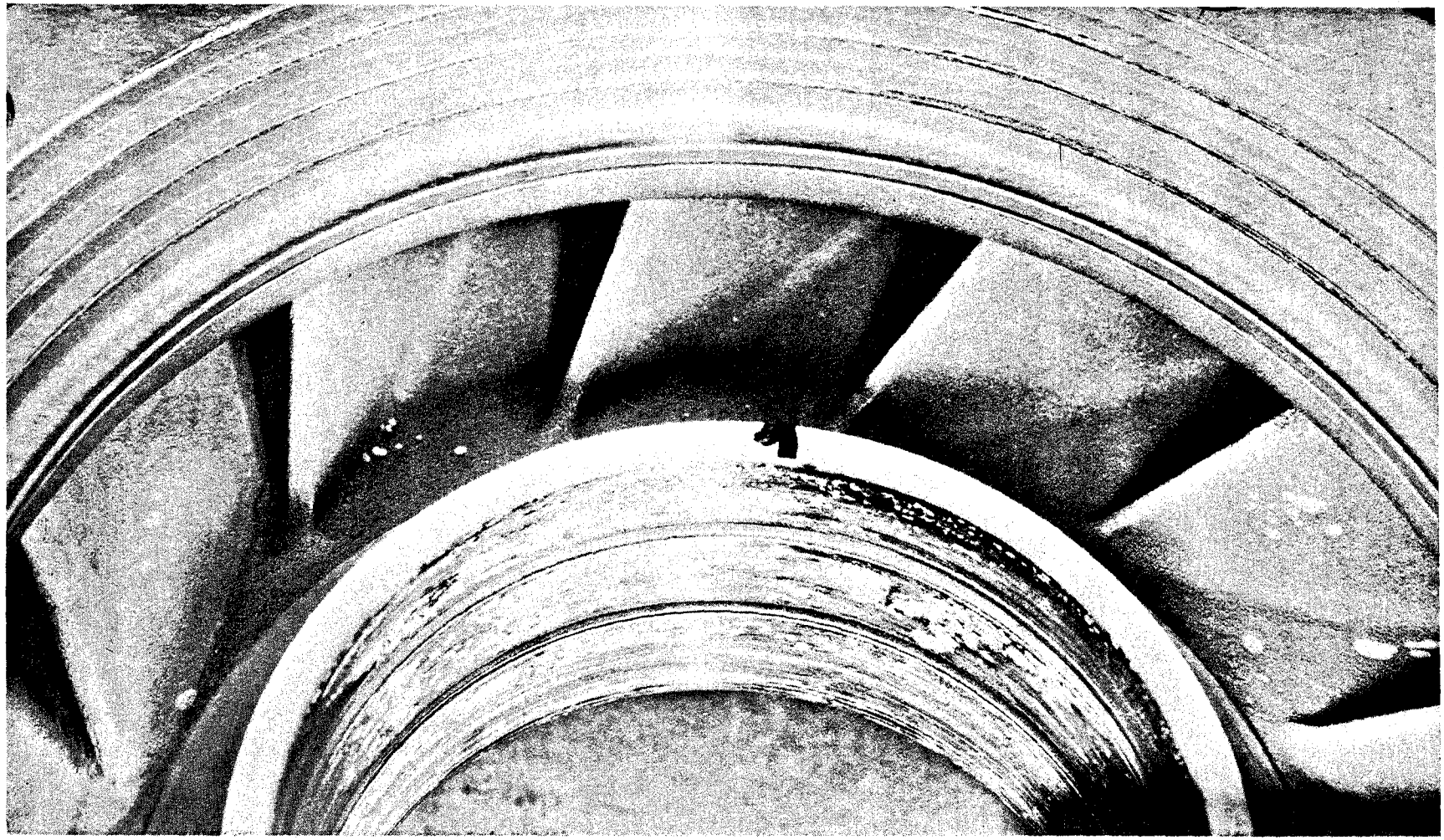

FIGURE 5. SPACE SHUTTLE MAIN ENGINE (SSME) HIGH PRESSURE FUEL TURBOPUMP (HPFTP) 0110R1 RUBBED IMPELLER INTERSTAGE SEAL STATOR

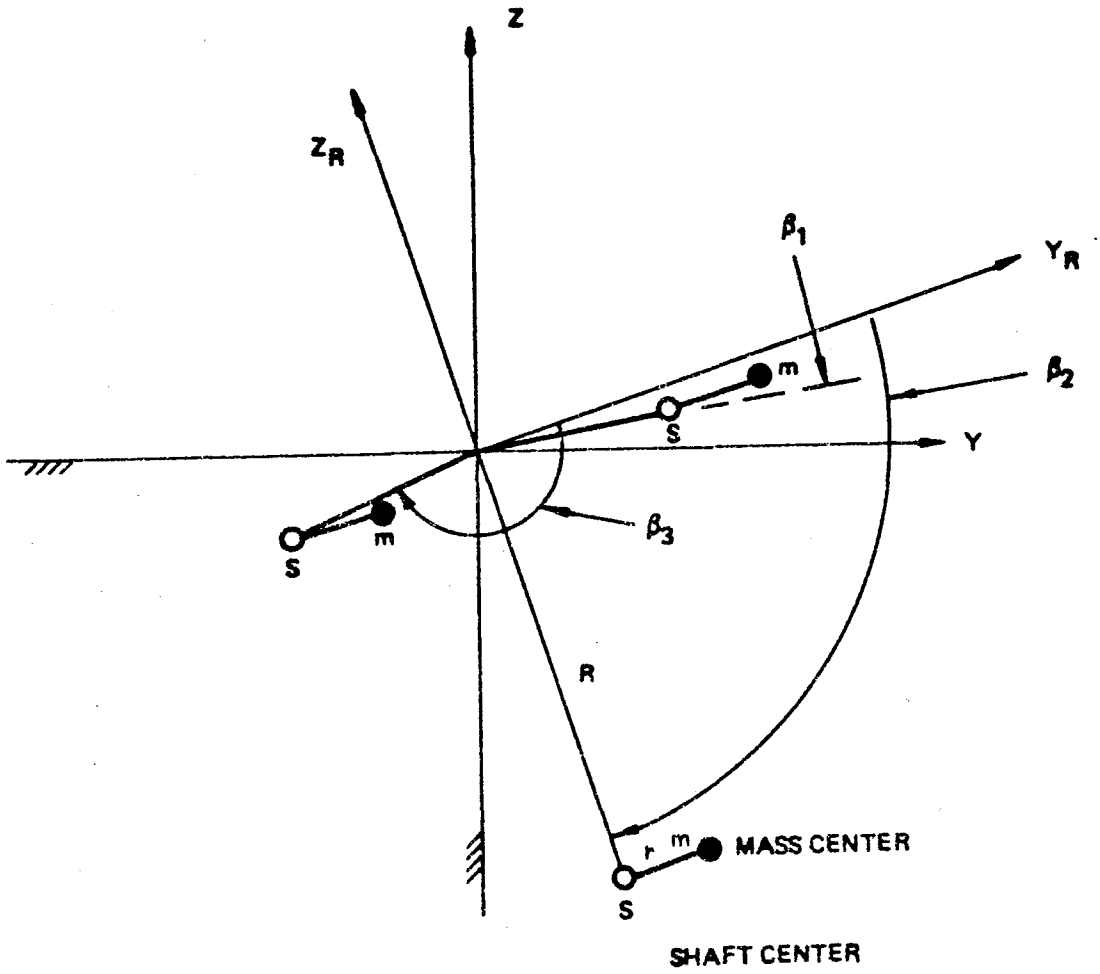

1) BELOW CRITICAL SPEED OPERATION β_1 : $\omega << \omega_c$ RUB ON HEAVY SIDE

2) AT CRITICAL SPEED OPERATION β_2 : $\omega = \omega_c$

3) ABOVE CRITICAL SPEED OPERATION β_3 : $\omega >> \omega_c$ RUB ON LIGHT SIDE

THERMAL BOW WOULD AMPLIFY UNBALANCE RESPONSE OF CASE 1 AND ATTENUATE CASE 3 SYNCHRONOUS.

FIGURE 6. SHAFT CENTER/MASS CENTER PHASE RELATIONSHIPS

EXPERIENCE BASE

Based on personal experience of correlating high frequency dynamic data with hardware inspections of rocket engine turbomachinery, it is hypothesized that partial contact steady state rubbing generates integer harmonic frequencies of the synchronous speed. This harmonic response is usually produced with a decreasing amplitude for an increasing harmonic number. Two and three times the synchronous frequency are generally the strongest harmonics. Response content for benign contact above the fourth harmonic is usually too small in magnitude to detect with respect to the instrumentation noise floor.

Additional observations based on test data from lightly damped rotors in high speed rotating turbomachinery with tight operational ball bearing clearances and monitoring housing mounted accelerometers include:

1) Rubbed rotor hardware which did not experience subsynchronous oscillations during operation (benign contact) is usually worn over about a 135° arc.
2) Rotating hardware from a turbopump which as experienced subsynchronous oscillations is always rubbed over the entire circumference.
3) Strong subsynchronous response operation usually does not produce the higher harmonics at significant amplitudes. However, the sum of half speed oscillations and the synchronous frequency may be present.
4) Harmonic amplitudes can be distorted by transmission through the housing making it difficult to locate the

exact rub location.

A rotor rubbing detection method is complicated for rotating machinery which must rely on housing mounted instrumentation, such as the rocket engine turbomahcinery of observation 4). Close-coupled rotor instrumentation in this application may be limited due to accessibility, compatibility with propellants and severe temperature environments. The housing transmission effects can be accounted for with an indepth correlation of hardware condition and dynamic data response characteristics.

III. THEORETICAL

ASSUMPTIONS

The correlation attempted herein between rotor rub arc and harmonic frequency generation is based on a gradually developed rub condition. That is, for example, rubbing which is not the result of a step unbalance, such as a turbine blade loss. A steady state condition and perfectly circular rotor and stator cross-sections are assumed. Also, the housing is assumed rigid.

MATHEMATICAL MODEL

The frequency spectrum produced by the rubbing contact over a portion of rotor circumference will be calculated by taking a Fourier series expansion of the assumed shaft motion of Figure 7.

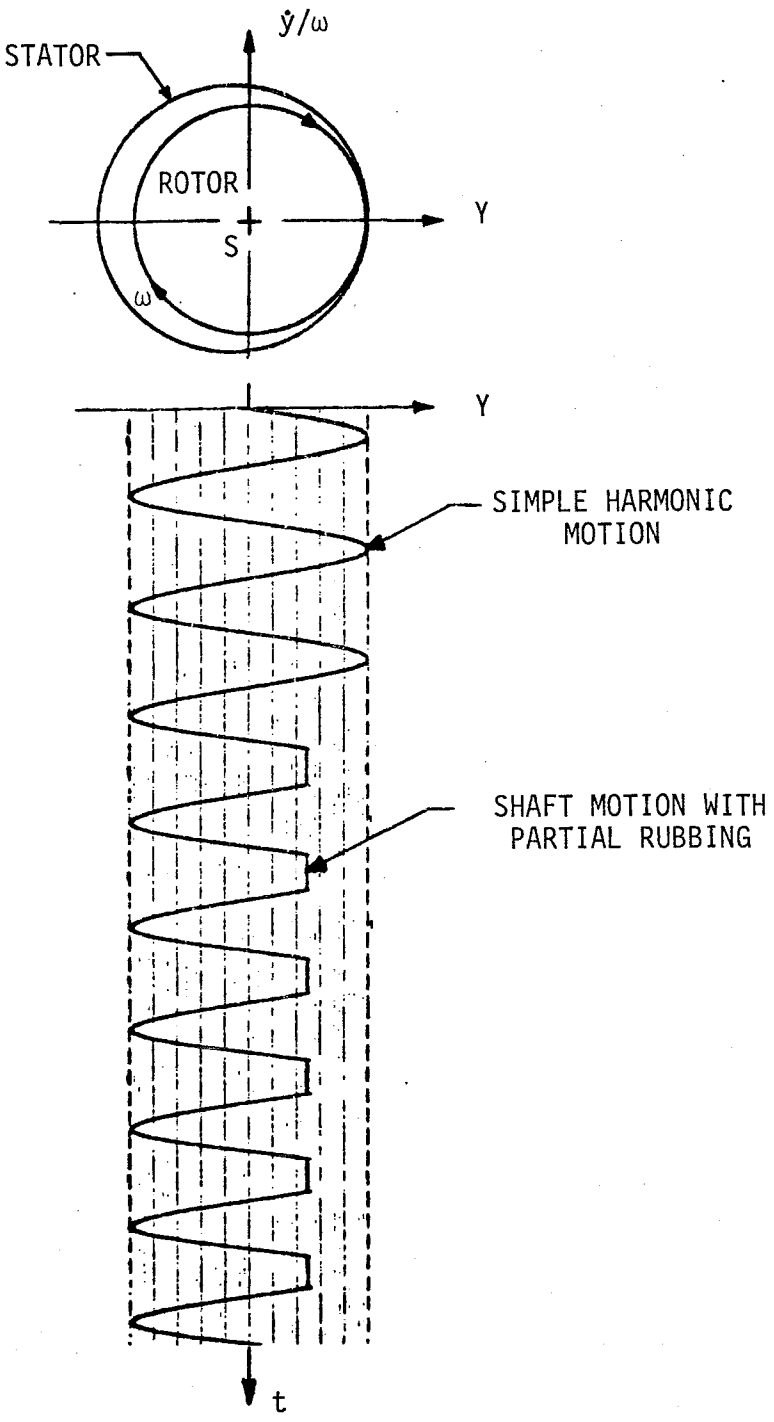

FIGURE 7. ROTOR RUBBING TIME HISTORY

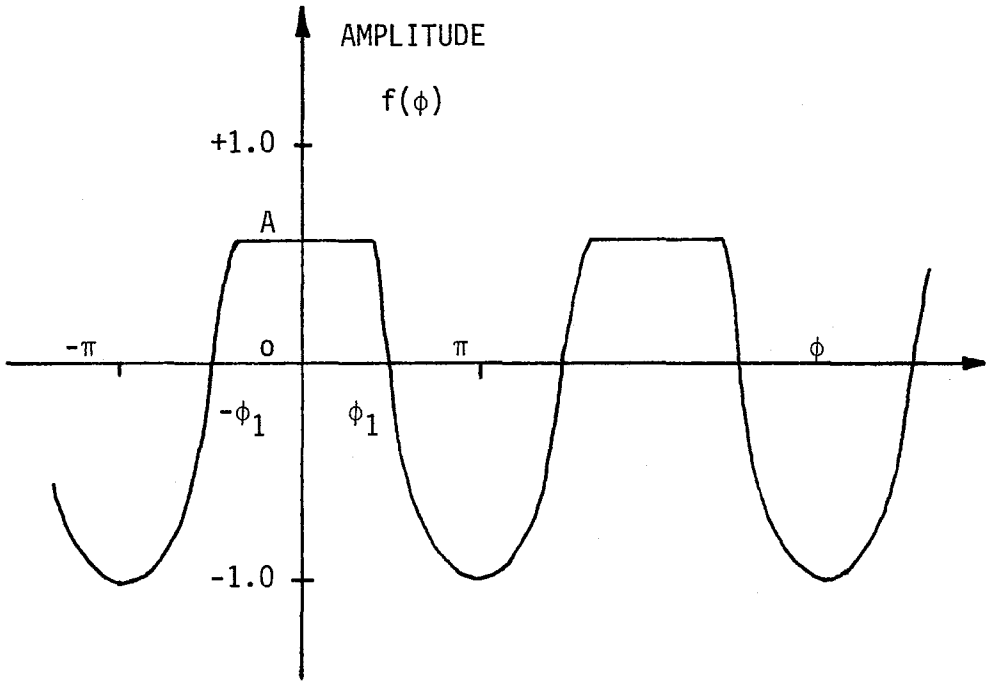

FIGURE 8. ASSUMED SHAFT MOTION

The rotor comes in contact with the stator once per revolution. The resulting shaft motion is shown in Figure 8. One complete revolution of the rotor represents one complete cycle. The resulting wave form, varying in amplitude from A to -1.0, is defined as:

$$f(\phi) = A \quad \text{for } -\phi_1 \leq \phi \leq \phi_1$$

$$f(\phi) = \cos\phi \text{ for } \phi_1 \leq \phi \leq -\phi_1$$

Where A is the truncated amplitude of the rotor response and ϕ is angular position. The Fourier series describing the complete rotor response is:

$$F(\phi) = \frac{a_o}{2} + \sum_{n=1}^{\infty} (a_n \cos n\omega t + b_n \sin n\omega t)$$

where $a_o/2$ represents the average static value of $F(\phi)$. $f(\phi)$ is

an even function (i.e. $f(-\phi) = f(\phi)$) so $b_n = 0$. The Fourier series reduces to:

$$F(\phi) = \frac{a_o}{2} + \sum_{n=1}^{\infty} a_n \cos n\omega t$$

where: $a_n = \frac{2}{L} \int_o^L f(\phi) \cos n\phi d\phi$ For $\begin{matrix} L = \pi \\ A = \cos\phi_1 \end{matrix}$

The rotor response equals:

$$a_n = \frac{2}{\pi} \left[\int_o^{\phi_1} A \cos n\phi d\phi + \int_{\phi_1}^{\pi} \cos\phi \cos n\phi d\phi \right]$$

Summarizing the expansion results contained in Appendix A:

$$\text{Static Amplitude} = \frac{a_o}{2} = \frac{1}{\pi} \left[\phi_1 \cos\phi_1 - \sin\phi_1 \right]$$

$$\text{Synchronous Amplitude} = a_1 = 1 - \frac{\phi_1}{\pi} + \frac{\sin 2\phi_1}{2\pi}$$

$$\text{Harmonic Amplitudes} = a_n = \frac{2}{\pi} \left[\frac{\cos n\phi_1 \sin\phi_1}{(n^2 - 1)} - \frac{\sin n\phi_1 \cos\phi_1}{n(n^2 - 1)} \right]$$

where $n = 1,2,3.....$

The relative harmonic amplitude results normalized to $a_1 = 1.0$ are plotted versus half the rotor rub arc (ϕ) in Figure 9. The harmonics are normalized in this manner so that all rotating machinery can be compared relative to its own synchronous vibration on an equal basis. Thus one machine is not penalized with respect to another due to truncation of a higher unbalanced response. It is this truncation of the shaft motion which generates the higher harmonics, typical of a nonlinear system. The amount of truncation of the unbalanced response is the rubbing indication of the amount of contact and the amplitude of the harmonics.

These relative harmonic strengths of Figure 9 can be used as the

diagnostic information needed to predict the operating condition. For example, if a spectrum analysis indicates a certain harmonic content and relative strength, it can be correlated to a particular contact arc. This can be accomplished by correlating relative harmonic response amplitudes of the data to the predicted plotted response with the best rub arc fit. Thus interpreting Figure 9, as the harmonic amplitudes increase, the rubbing becomes more severe because more of the rotor circumference comes in contact under a perfectly circular rotor and stator condition. Tracking the vibration performance in this manner combined with other engineering data and judgement, the analyst can recommend maintenance at the proper time. Other engineering data may be the machine efficiency data, or torque checks, and judgements may be based on the experience of what has occurred when a similar machine indicated the same harmonic content.

This analysis also predicts synchronous unbalanced response as related to the arc of rotor rubbing. The synchronous response is determined from the Fourier series expansion of the rubbed wave shape for the n = 1 terms (a_1). The synchronous response as a function of half the arc of rotor rubbing is shown in Figure 10. It can be seen from Figure 10 that for small rub arcs the synchronous vibration is unchanged, and as the rotor rubbing arc becomes larger the synchronous vibration is attenuated. As the synchronous amplitudes decline, the harmonic amplitudes become more significant. This may be due to the rub location approaching behavior similar to a bearing and the rotor response decreases due to the additional support. In reality, the synchronous response may be somewhat different due to the previously described deadband, thermal and housing transmission effects.

Summarizing the theorized rubbing progression, initial contact causes decreased synchronous vibration and low level harmonics. As more of the rotor circumference begins to rub, the synchronous vibration amplitudes continue to decrease and the harmonic frequencies amplitudes increase, with the second and third harmonics the strongest. When the rotor rubbing location has a contact arc of 360°, the harmonic amplitudes disappear. The rotor is then likely to be unstable per the introductory description or it could possibly seize with the housing.

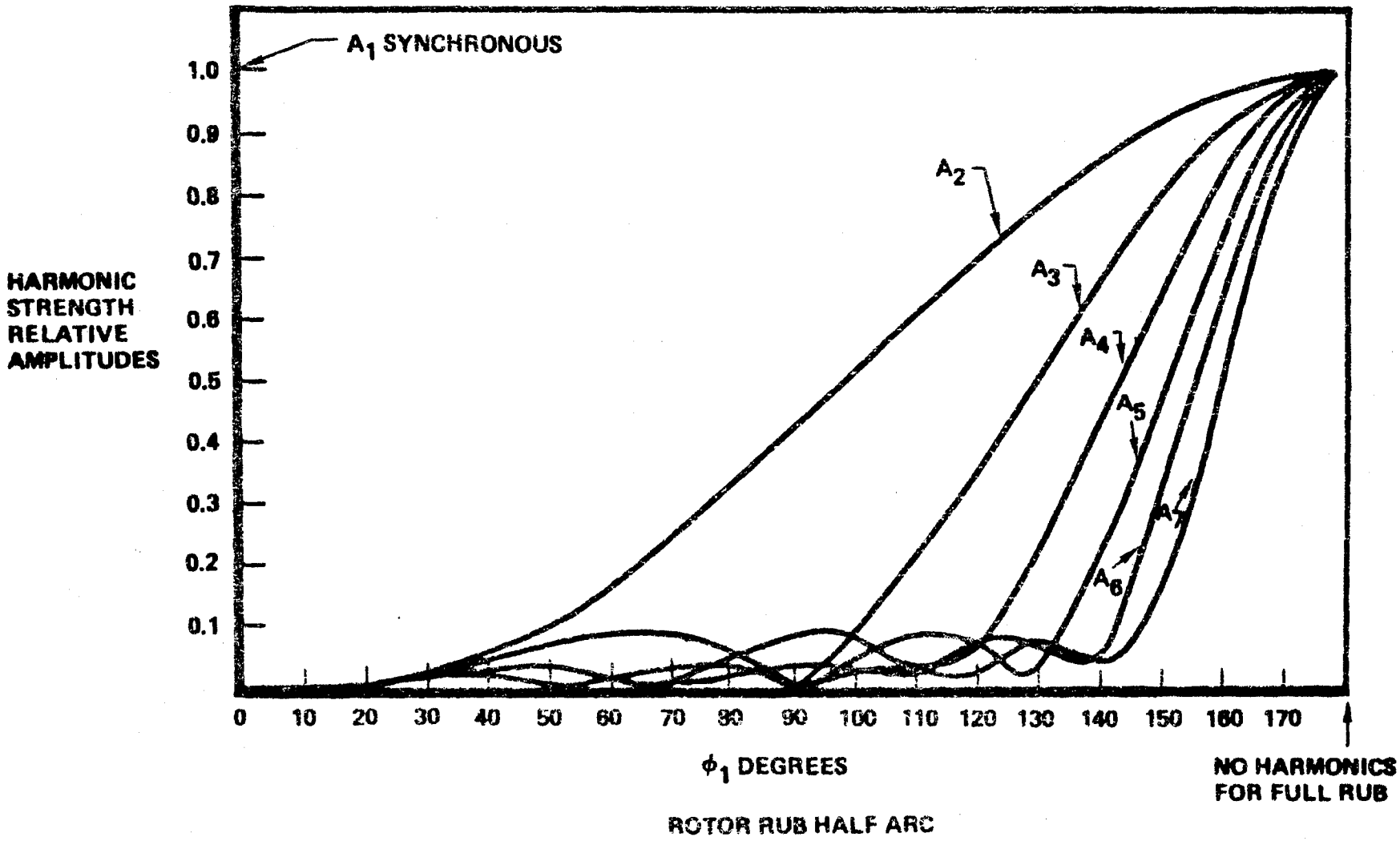

FIGURE 9. RELATIVE HARMONIC AMPLITUDES VERSUS HALF THE ROTOR RUB ARC

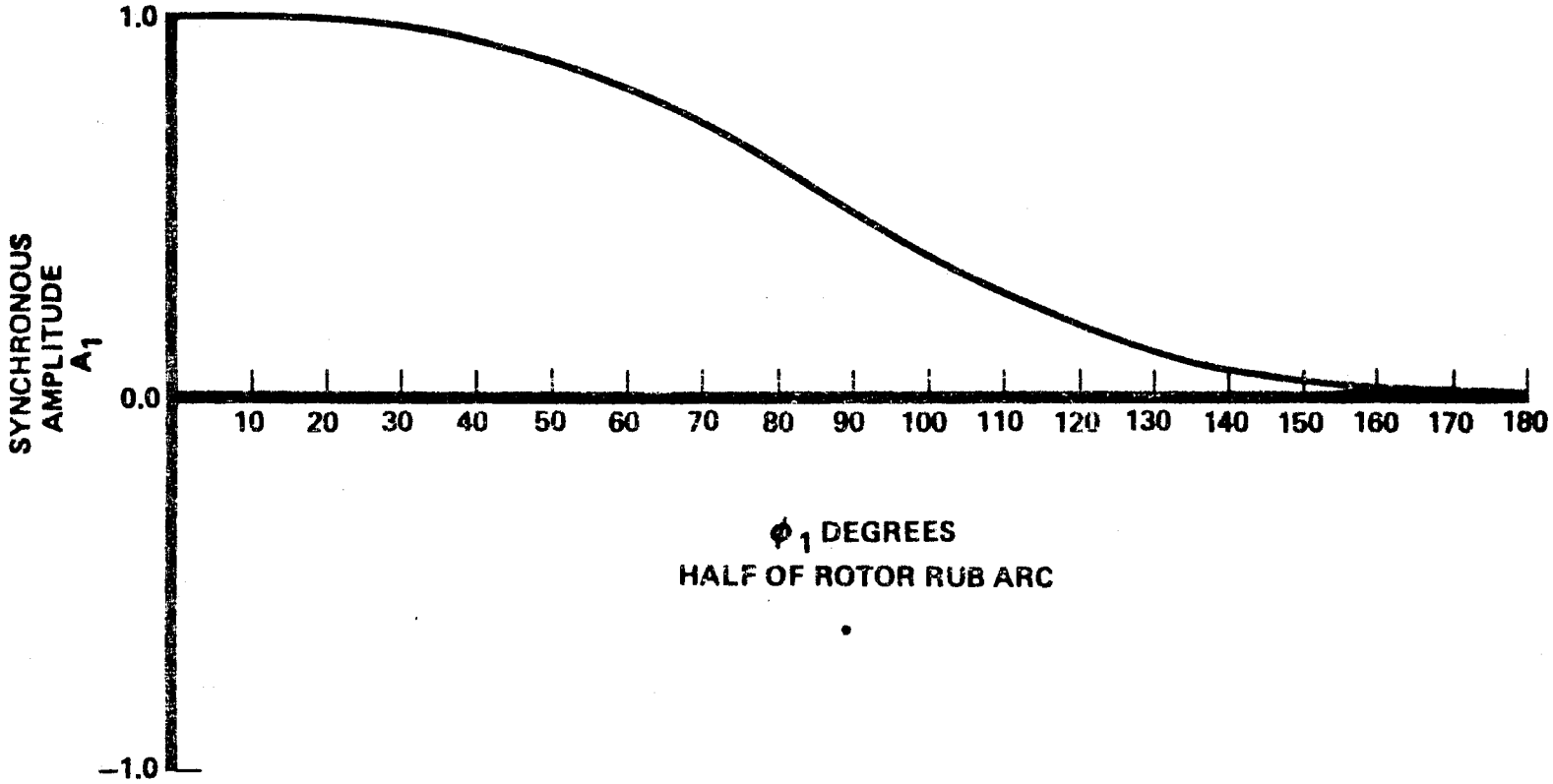

FIGURE 10. SYNCHRONOUS AMPLITUDE VERSUS HALF THE ROTOR RUB ARC

IV. EXPERIMENTAL

LABORATORY VERIFICATION

The rotor kit of Figure 11 was assembled similar to the Bently experiment, with bearing clearances as small as possible. The test configuration is shown in Figure 12. This assembly is representative of a typical rotor construction as opposed to the more commonly analyzed Jeffcott rotor. This configuration is analogous to a pumping disk (i.e., inducer or impeller) and a turbine disk straddled by bearings with a seal between the disks where the possibility of rubbing exist. The experiments were conducted in the Rocketdyne Analog Room facility using a Real Time Data Analyzer (RTDA) to perform the frequency spectrum analyses. The equipment, test rotor kit and experimental set up are shown in Figures 13 and 14. Appendix B contains a description of the data processing techniques and output format.

Summarizing the experimental procedure; a brass screw was tightened onto the steel shaft between the disks during steady state operation. Orthogonal displacement transducer output signals detecting rotor response were supplied to a dual beam oscilloscope for an orbit plot and a time history display. In addition, the signals were supplied to the RTDA for spectrum analysis. A block diagram of the system is shown in Figure 15.

In support of this experiment, a finite element model of the rotor was constructed as shown in Figure 12. Critical speeds and rotor mode shapes were calculated using techniques described in Reference (13). A critical speed versus support stiffness plot is shown in Figure 16, indicating the shaft is much more flexible than the supports. The rotor critical speeds are determined by shaft

flexibility in this case and are independent of the support stiffness. The rotor mode shapes are shown in Figure 17.

The oscilloscope pictures of Figure 18 were taken during a steady state rubbing operation. The rubbed shaft motion indicates the theorized shaft motion is a good approximation. Figure 19 shows the frequency response spectrum during this interaction and indicates harmonic frequency generation up to the fifth harmonic. The vertical displacement transducer response indicated higher harmonic amplitudes in the direction of the rubbing. An amplitude spectrum indicating the relative strength of the harmonic is shown in Figure 20. Spanning the frequency spectrum analysis to 500 Hz (to include only the fifth harmonic) and varying the shaft speed to simulate a ramping condition, produces the synchronous and harmonic tracking trend shown in Figure 21. If the rubbing is increased until the screw is in contact with the rotor over the entire circumference while operating well above the critical speed, a rotor stability at a frequency near the rotor critical speed is driven as shown in the oscilloscope picture of Figure 22, and isoplot of Figure 23. The instability frequency is close to the calculated critical speed of the rotor assuming a stiffening effect of the screw support. The rubbing condition critical speeds map is plotted in Figure 24 and the rotor mode shapes are shown in Figure 25. This result matches the Ehrich (6) earlier contention.

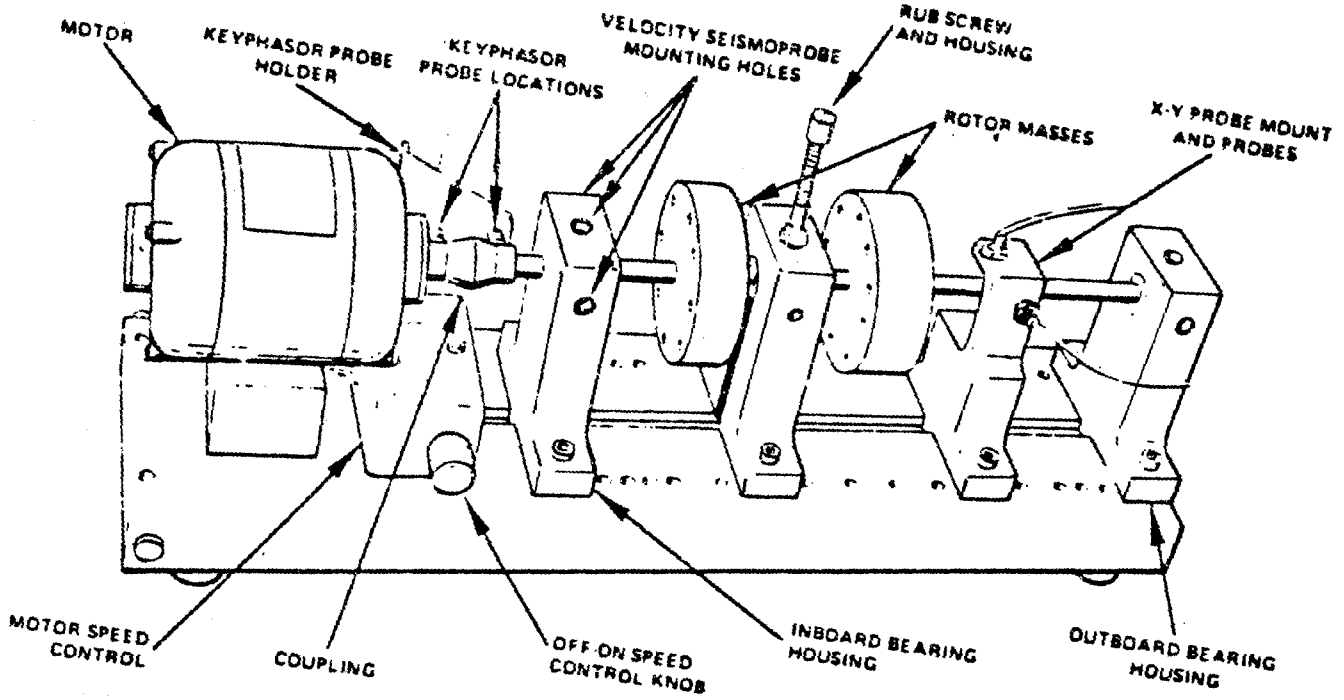

FIGURE 11. BENTLY ROTOR KIT MODEL 24750

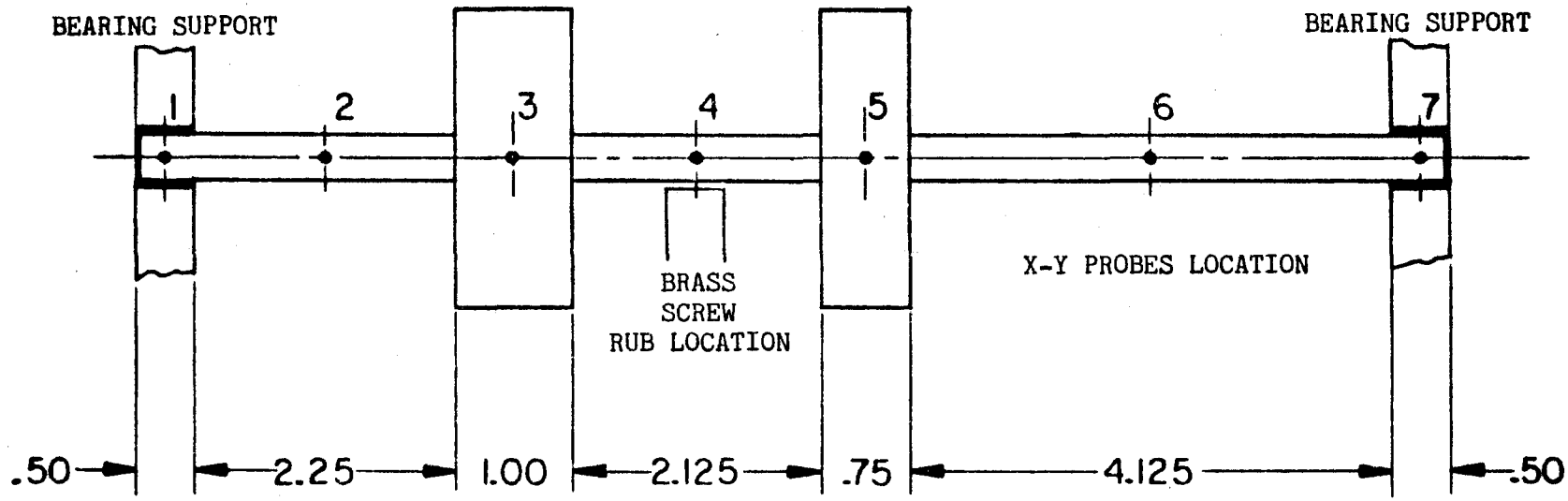

● FINITE ELEMENT MODEL JOINT LOCATION

FIGURE 12. TEST ROTOR KIT DESCRIPTION/MODEL

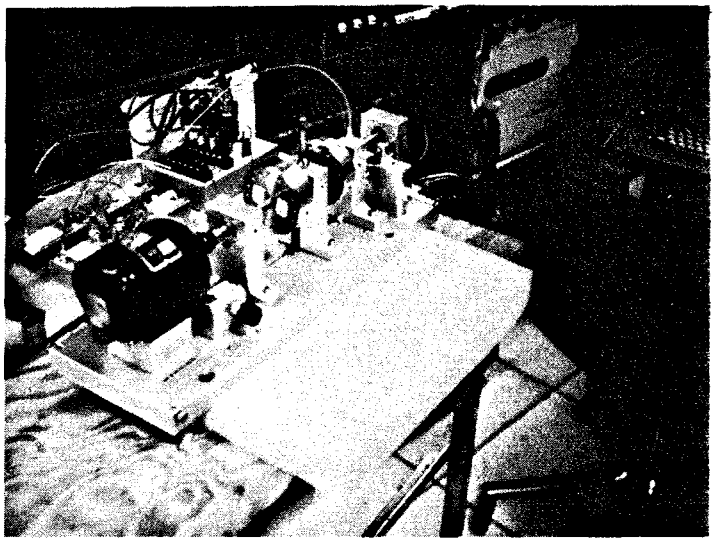

FIGURE 13. EXPERIMENTAL SETUP - PHOTOGRAPHS 1 AND 2

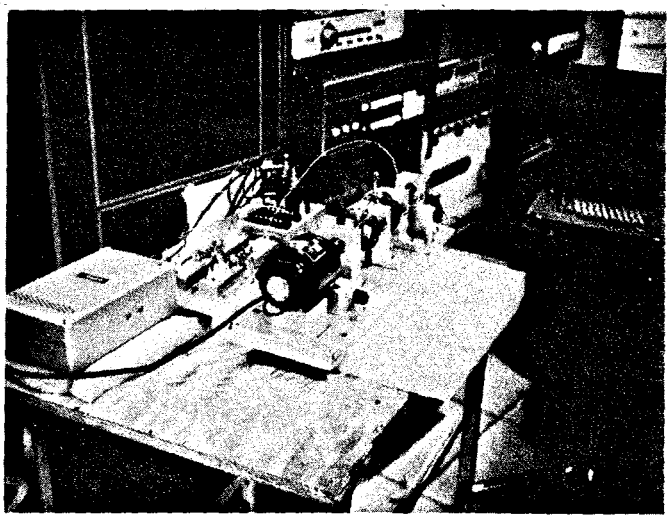

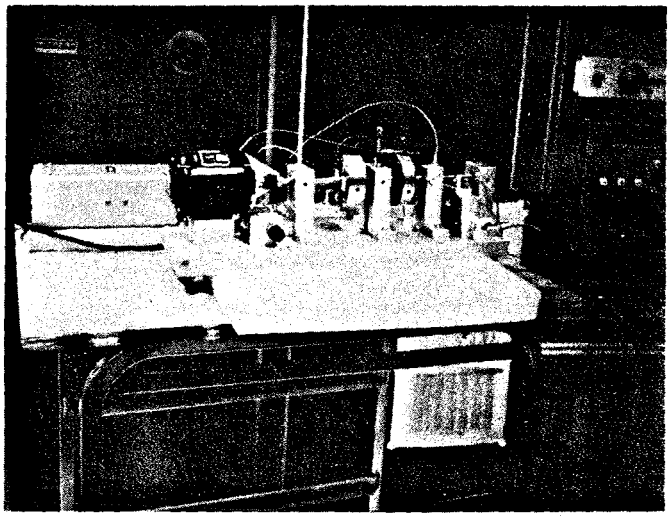

FIGURE 14. EXPERIMENTAL SETUP - PHOTOGRAPHS 3 AND 4

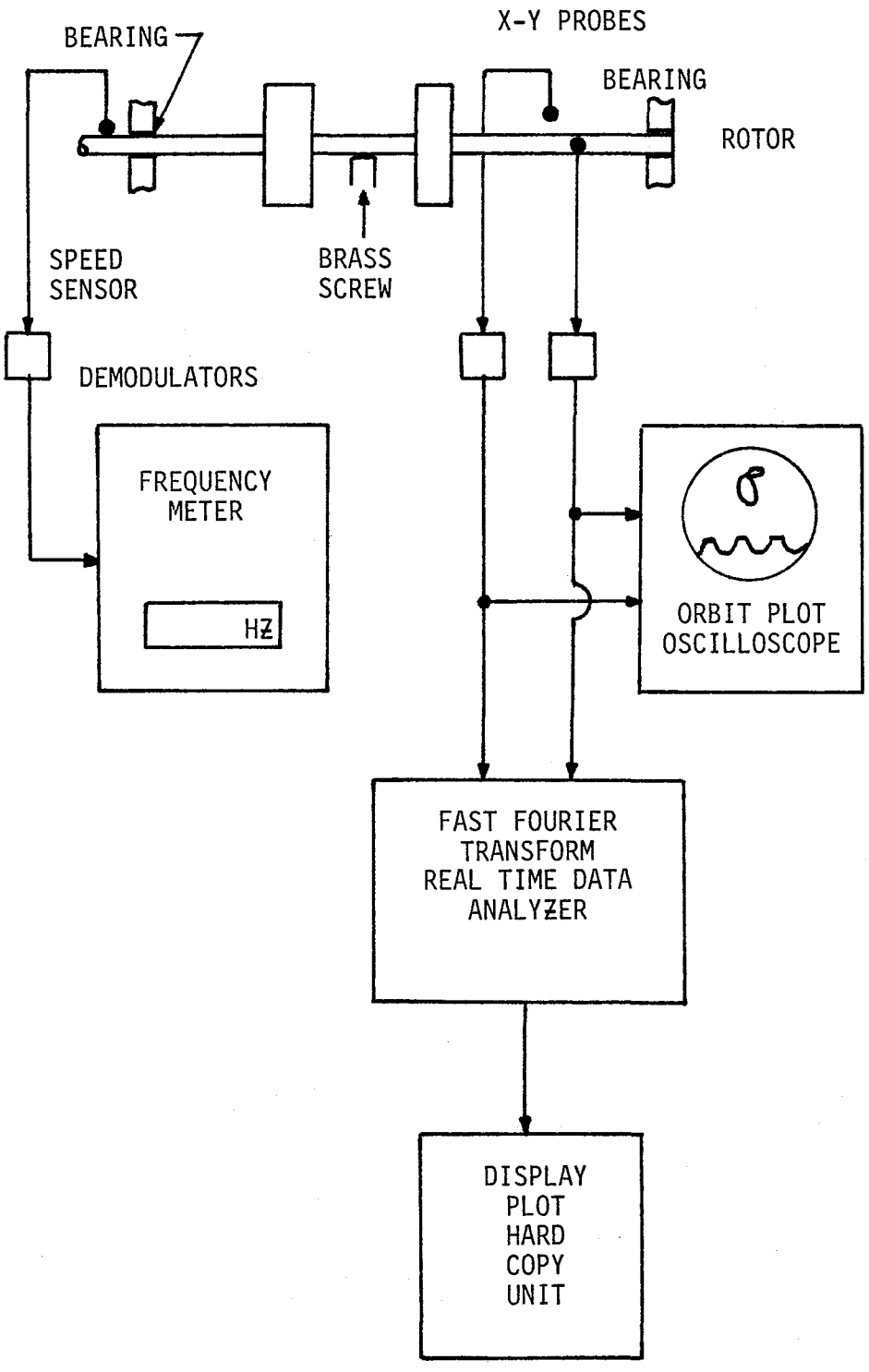

FIGURE 15. BLOCK DIAGRAM OF INSTRUMENTATION

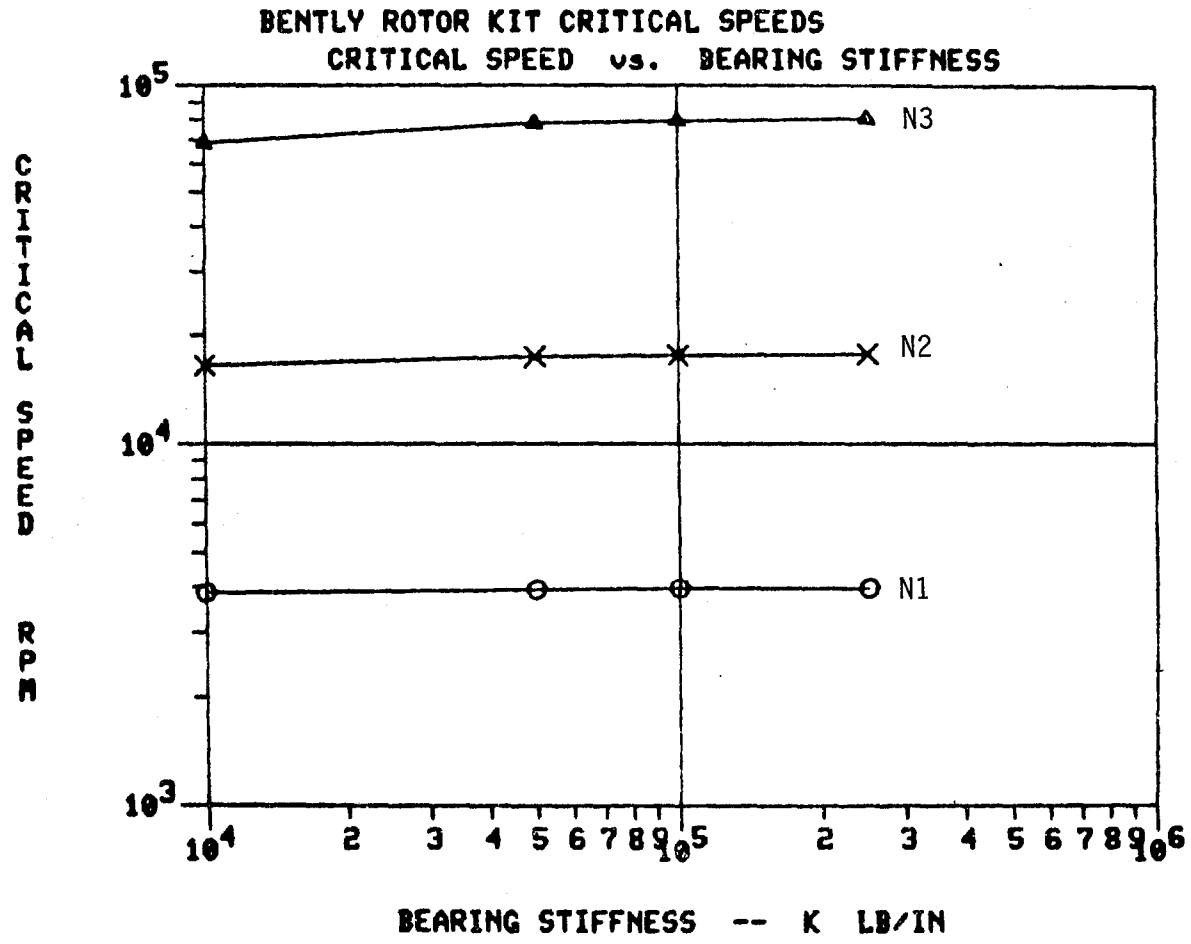

FIGURE 16. ROTOR KIT CRITICAL SPEEDS VERSUS BEARING STIFFNESS

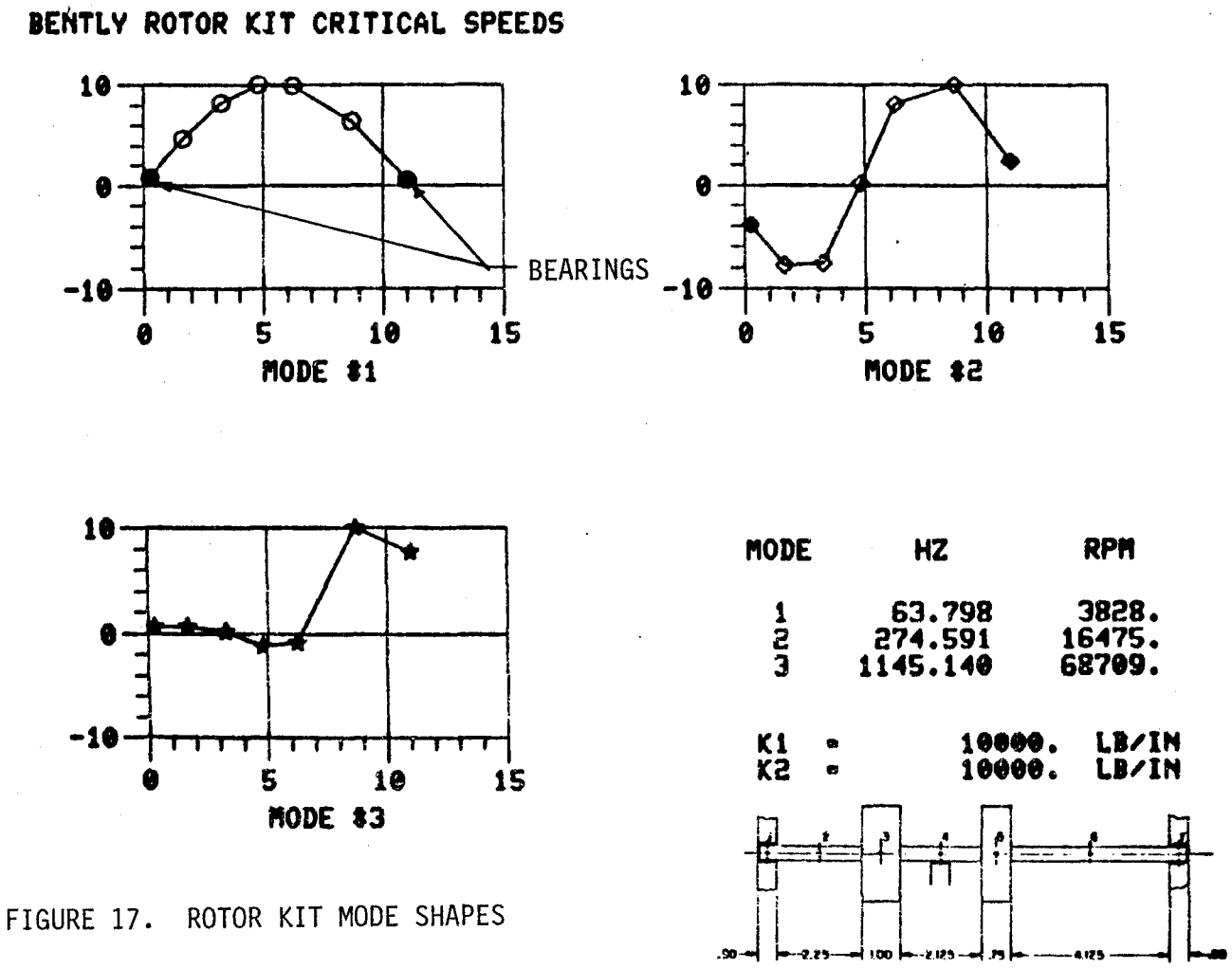

FIGURE 17. ROTOR KIT MODE SHAPES

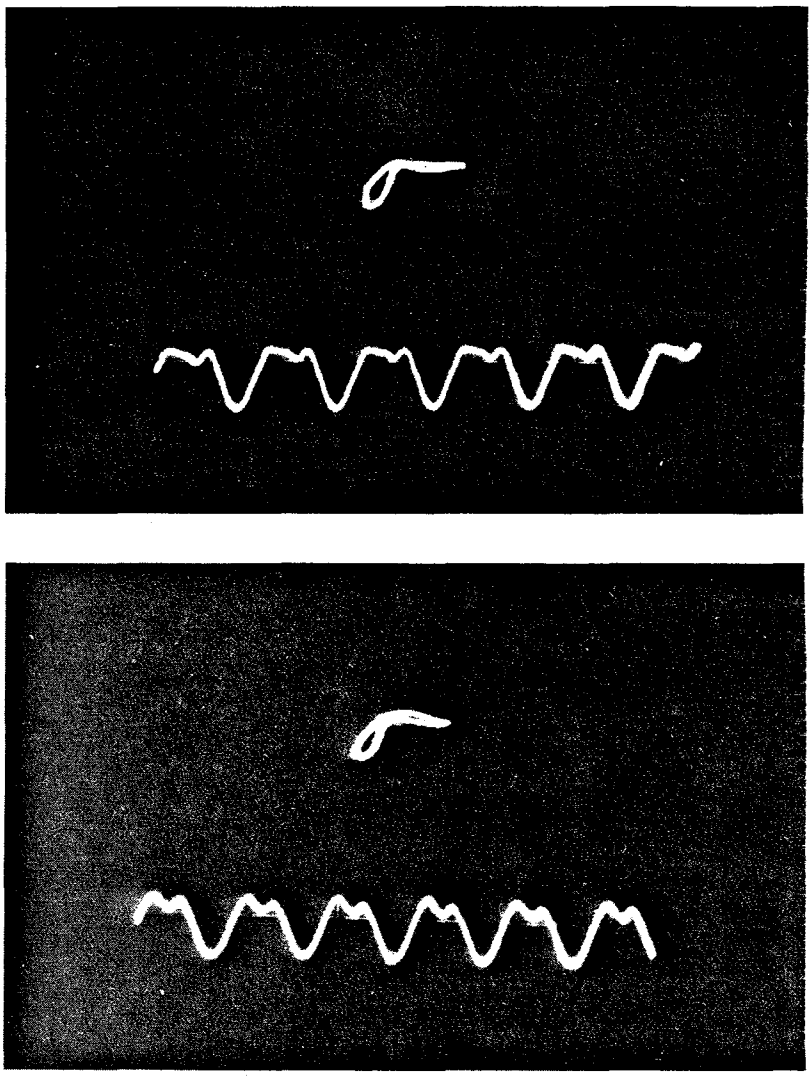

FIGURE 18. ROTOR KIT PARTIAL RUBBING RESPONSE ORBIT PLOTS AND TIME HISTORY OSCILLOSCOPE PHOTOGRAPHS

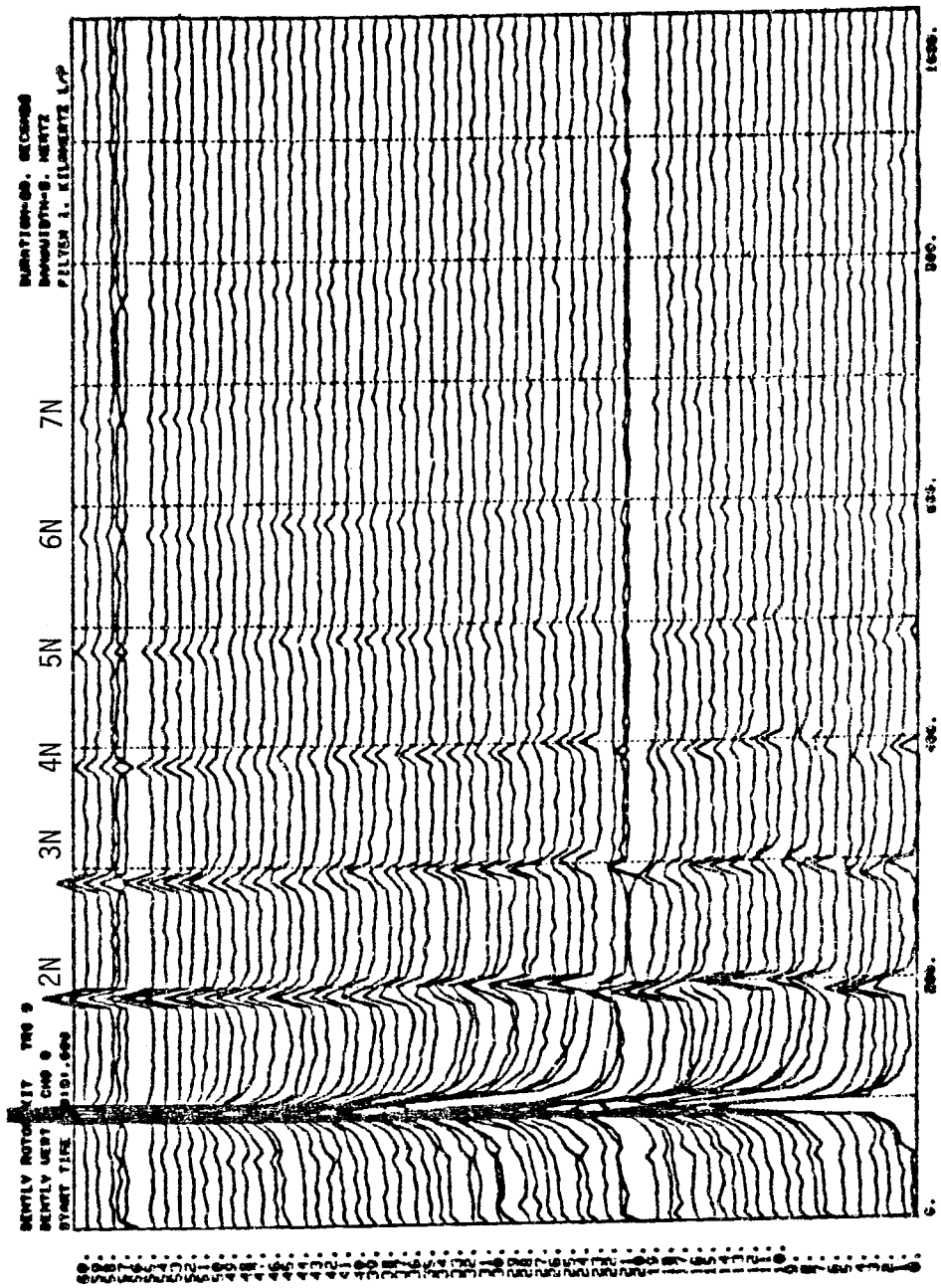

FIGURE 19. ROTOR KIT STEADY STATE RUBBING RESPONSE FREQUENCY VERSUS TIME

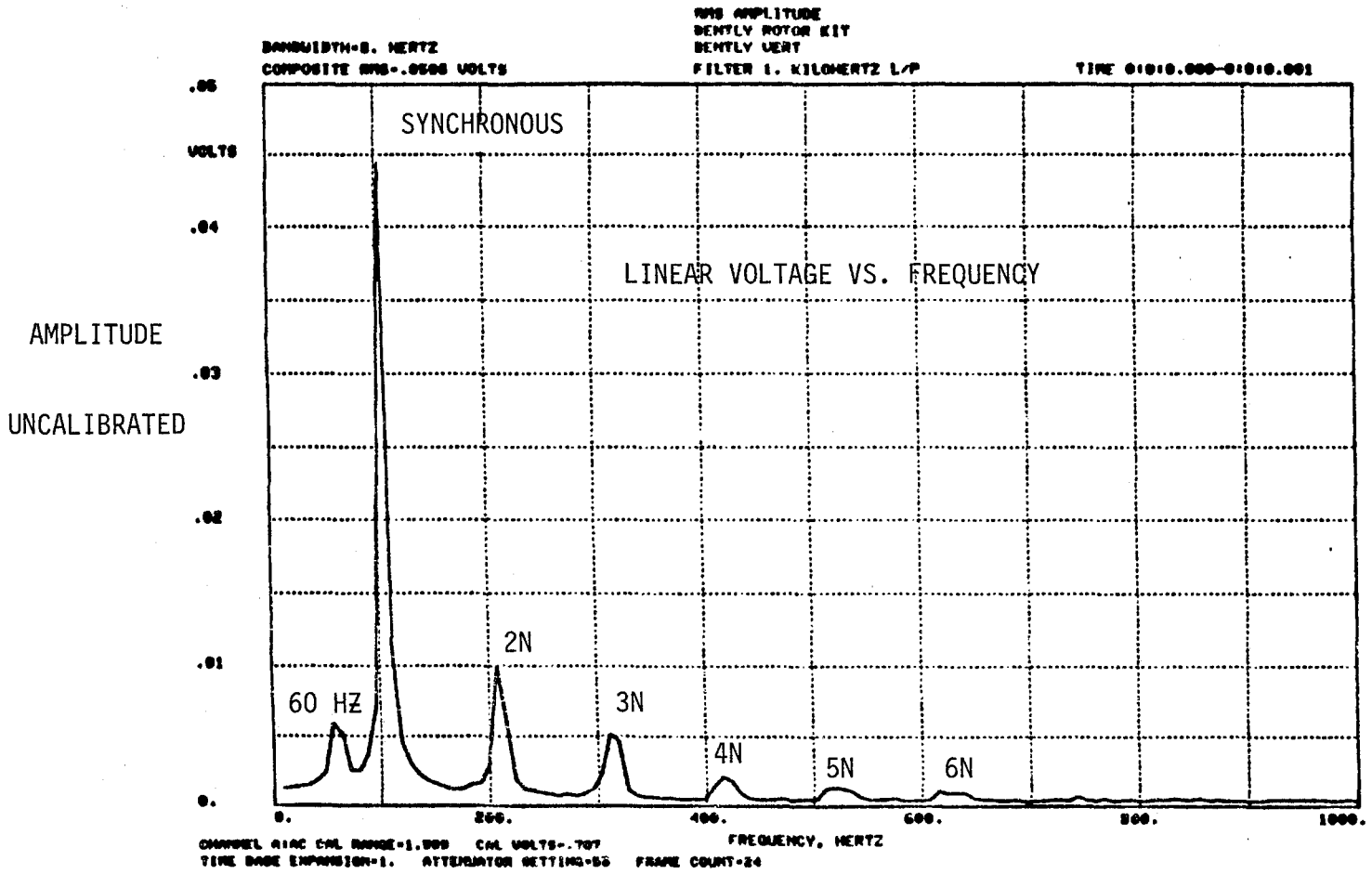

FIGURE 20. ROTOR KIT RUBBING RESPONSE SPECTRAL ANALYSIS

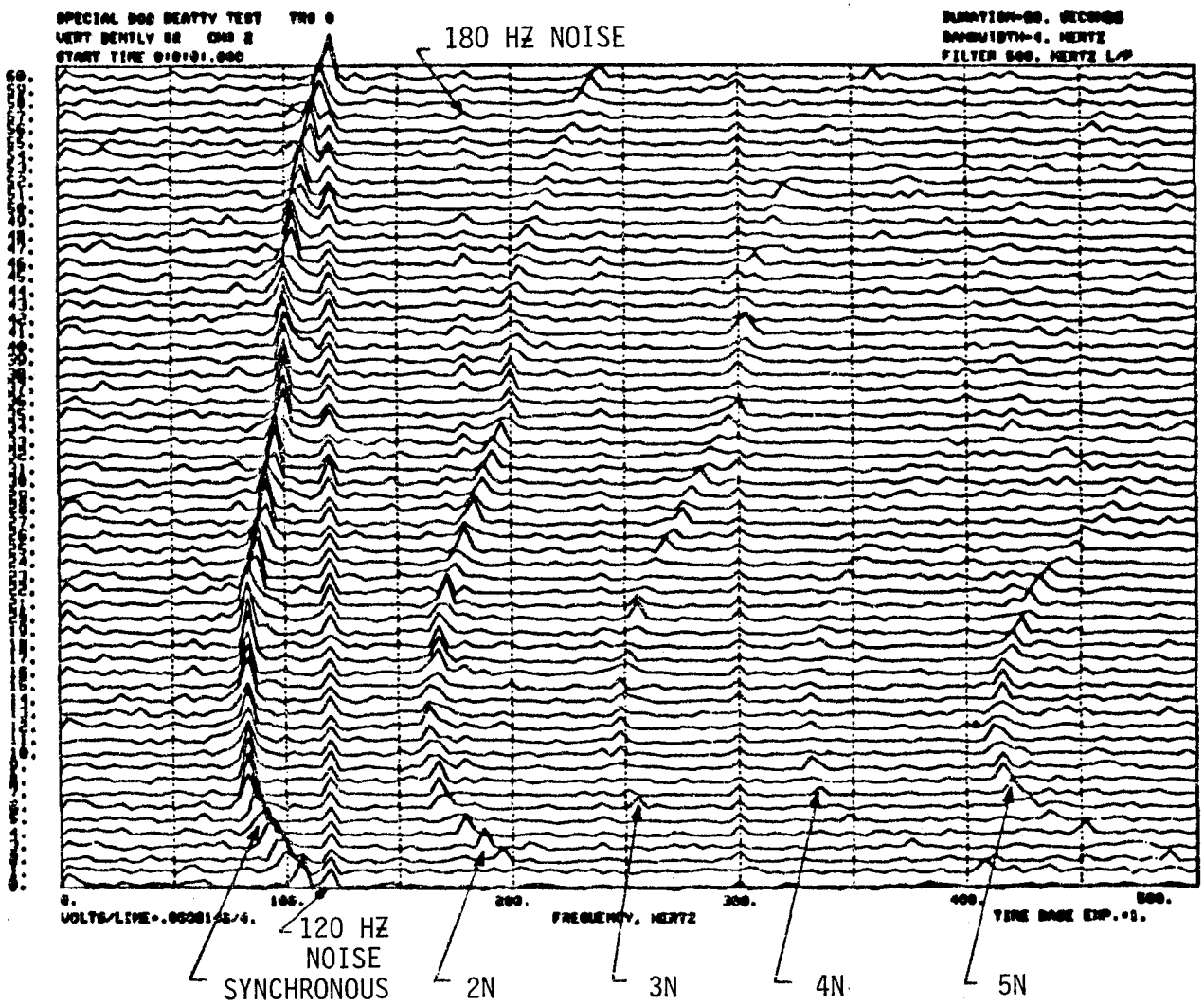

FIGURE 21. ROTOR KIT TRANSIENT RUBBING RESPONSE FREQUENCY VERSUS TIME

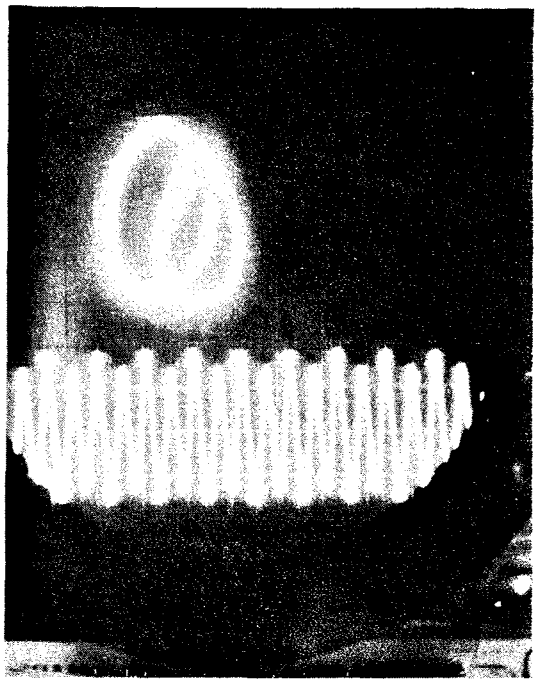

FIGURE 22. ROTOR KIT RUBBING INSTABILITY ORBIT PLOT AND TIME HISTORY PHOTOGRAPH

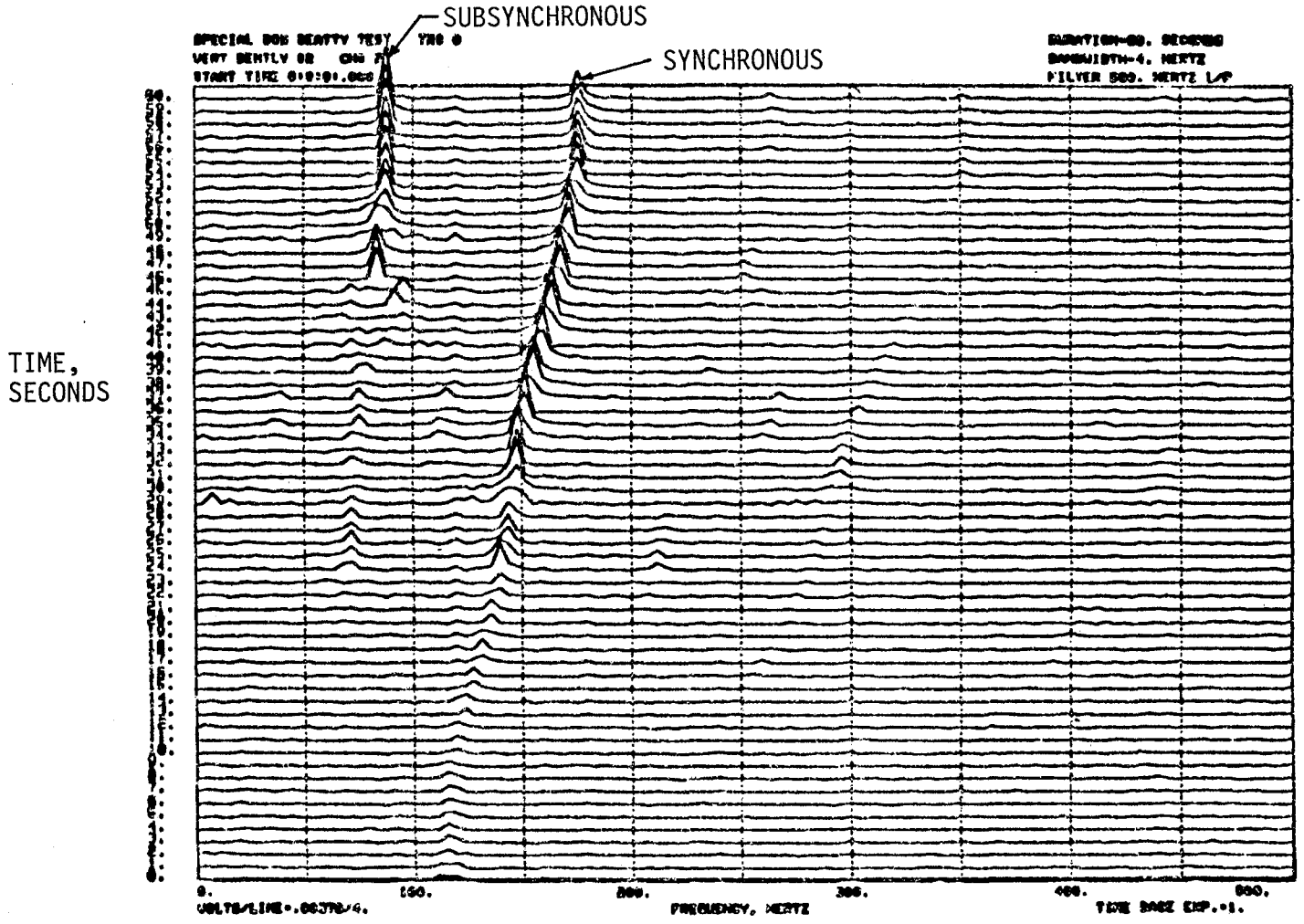

FIGURE 23. ROTOR KIT SUBSYNCHRONOUS RUBBING INSTABILITY FREQUENCY VERSUS TIME

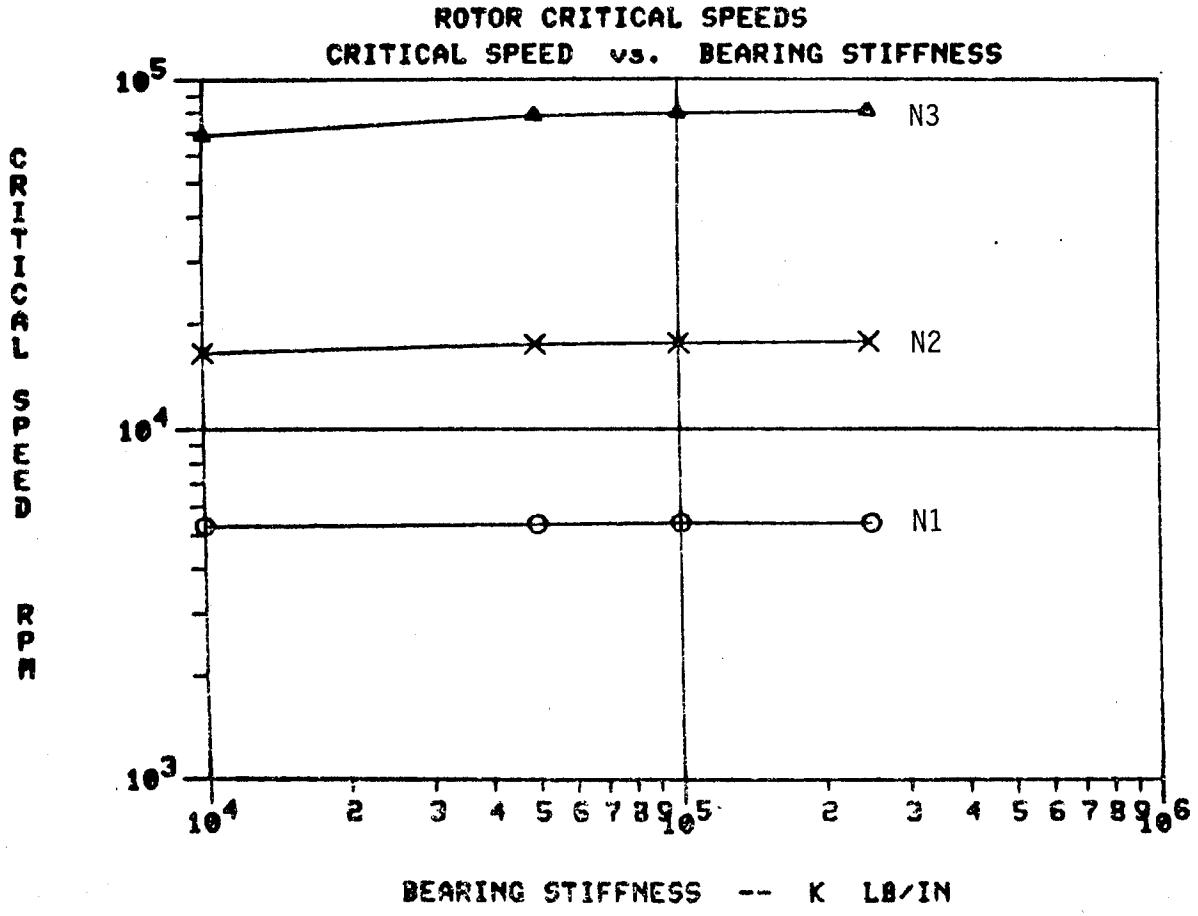

FIGURE 24. ROTOR KIT CRITICAL SPEEDS VERSUS BEARING STIFFNESS FOR RUBBING CONDITION

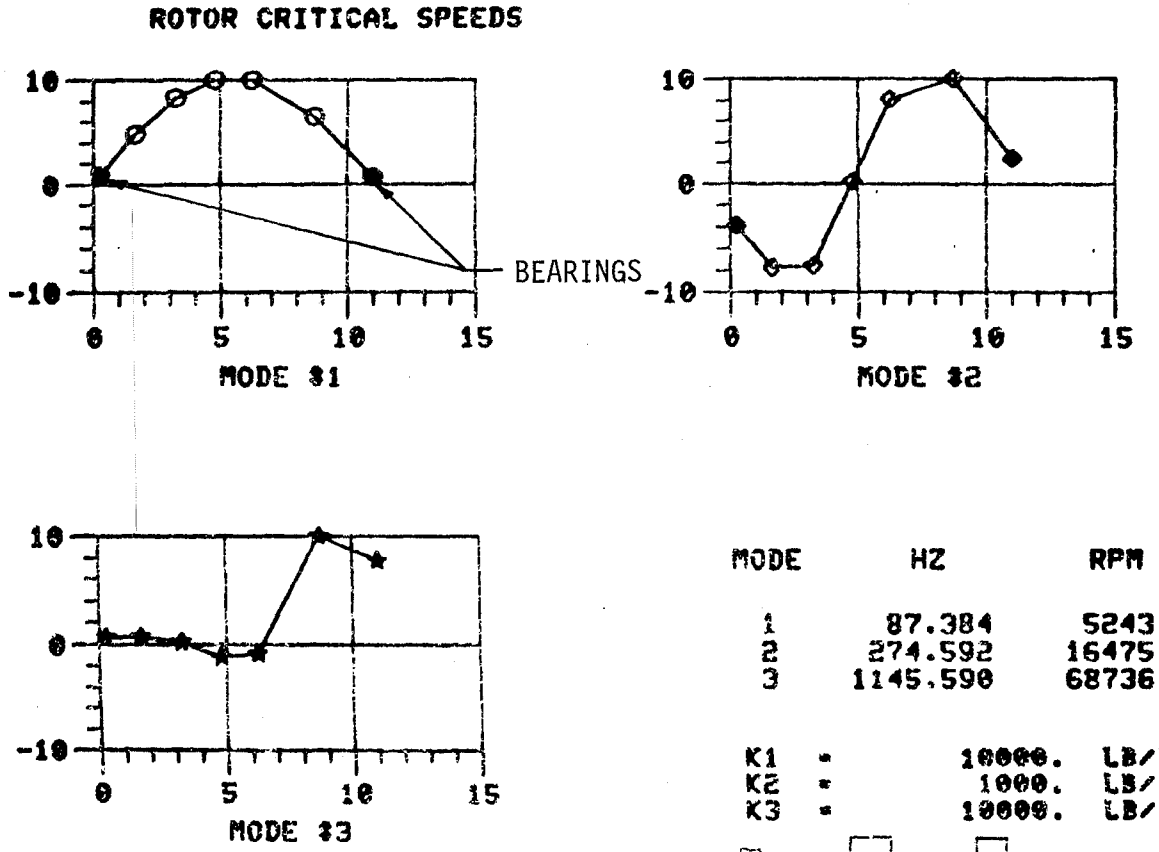

FIGURE 25. ROTOR KIT MODE SHAPES FOR RUBBED CONDITION

INDUSTRY EXAMPLES

The Low Pressure Fuel Turbopump (LPFTP) of the Space Shuttle Main Engine (SSME) has a direct drive rotor with a rated power level speed of approximately 15,500 RPM. A description of the machine and a cross-section of the turbopump is shown in Figure 26. The rotor first critical speed is approximately 22,500 RPM.

LPFTP unit number 82402 experienced approximately 1400 seconds of high power level testing. During operation, harmonic frequencies were measured by externally mounted housing accelerometers located on the turbine flange. The typical wave form is shown in Figure 27 and the response spectrum is shown in the frequency versus time plot of Figure 28. During normal turbopump operation only synchronous response, due to rotor unbalance, and four times speed inducer blade wake response are present. The high level harmonic frequency response, particularly at two and three times speed, are anomalous. An amplitude versus frequency plot is shown in Figure 29 during steady state operation indicating the strength of the synchronous and harmonic frequencies as measured on the turbine end housing. Disassembly of this turbopump (Tepfer (14)) revealed the turbine seal rubbed over a rotor arc of 135° as the only significant anomally since the turbine seal normally does not rub. The inspection results are summarized in Figure 30. This example was chosen for this undisputable source and response relationship.

Monitoring of synchronous vibration levels as an indicator of rotor rubbing can be inconsistent and unreliable. This is due to the

possible combination of many other variables which affect synchronous unbalanced response. Some examples of changing unbalance are: spalling turbine blade coating, trapped fluid cavitation, pilot slipping and thermal bow. In some cases machines which have experienced rubbing produce high synchronous levels, while in others this may not be the case. Examples of a varying synchronous vibration amplitude at a constant rated power level speed and different interpretations are shown in the data from the Space Shuttle Main Engine (SSME) High Pressure Fuel Turbopump (HPFTP), shown in Figure 31. The monitoring accelerometer location is shown in the half section view of Figure 32. Tracking filter and spectral data from two different units are shown in Figures 33 and 34. Review of the data, using the techniques presented, indicates the turbopump of Figure 33 is rubbing when the synchronous vibration amplitudes are low. At this time the rotor response has subsynchronous oscillation amplitudes at the first critical speed frequency in the spectral data due to rubbing. In comparison, the turbopump of Figure 34 is rubbing when the synchronous vibration amplitudes are high. At this time the second harmonic response amplitude increases. The turbopump of Figure 33 was rubbed at the seal shown in Figure 4 over the entire circumference. The turbopump of Figure 34 was rubbed over approximately 120° arc at the same seal. This data correlation agrees with the predicted response and with what was observed in the rotor kit testing.

Detection of full contact radial rubbing for the case of an insufficient frictional cross-coupling force to cause a backward whirl instability and no harmonic frequency generation can be accomplished

by plotting the path of the rotor precessional motion. This technique consists of creating an orbit plot from digitized phase correlated data. Orthogonal measurements and knowledge of the rotor spin direction are required. An orbit plot of backward synchronous precession is indicative of full radial rubbing. An example of this phenomenon is depicted in the orbit plot of Figure 35 from HPFTP accelerometer data. This plot demonstrates precessional motion counter to the spin direction.

The HPFTP has a unique operating situation in that the turbine end bearing is not cooled with liquid hydrogen until after the engine is started. It usually requires approximately six seconds after start for the bearing to chill to the operating conditions of a tight clearance. This provides a situation where the rotor response can be evaluated with a varying bearing deadband. Figure 36 shows a frequency versus time plot of a HPFTP start to mainstage operation. Subsynchronous, synchronous and the sum frequencies are present from just before the shaft speed reaches steady state to approximately +6.4 seconds. This indicates that oscillations at half speed are associated with the bearing deadband and identified as deadband whirl. The sum frequency is present per the contention of Ehrich (8).

LOW PRESSURE FUEL TURBOPUMP

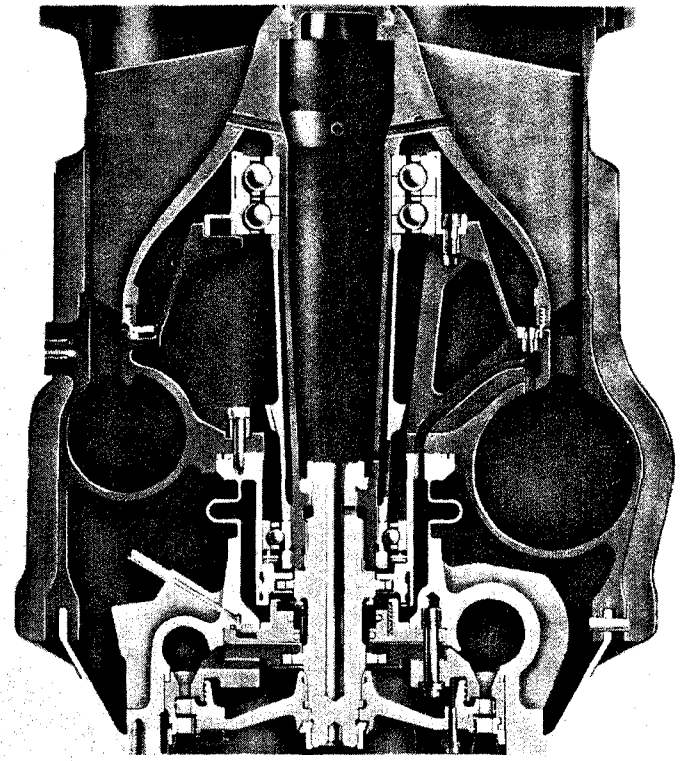

KEY PERFORMANCE PARAMETERS	RPL	FPL
PUMP INLET FLOWRATE LB/SEC	147.9	161.1
PUMP INLET PR PSIA	30.0	30.0
PUMP DISCH PR PSIA	261.8	282.6
PUMP EFFICIENCY	.674	.679
TURBINE FLOWRATE LB/SEC	28.7	32.2
TURBINE INLET TEMP R	459.	455.
TURBINE PRESSURE RATIO	1.30	1.32
TURBINE EFFICIENCY	.536	.530
TURBINE SPEED RPM	15370.	16249.
TURBINE HORSEPOWER	3003.	3536.

FIGURE 26. SPACE SHUTTLE MAIN ENGINE (SSME)
LOW PRESSURE FUEL TURBOPUMP (LPFTP)

LPFTP TURBINE FLANGE RADIAL ACCELEROMETER 180°

TEST: 750-100-0282

42.5 G_{pp} FULL SCALE

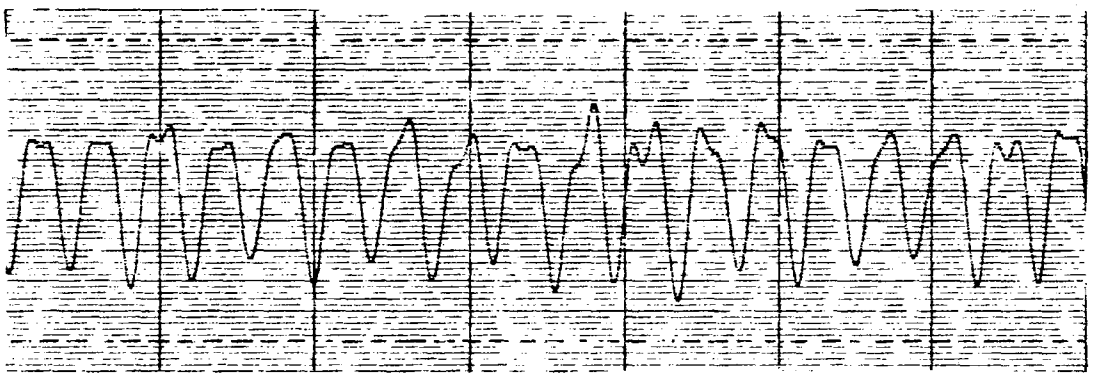

ONE SIDED TRUNCATED WAVE SHAPE FORM

2500 HZ LOW PASS FILTERED

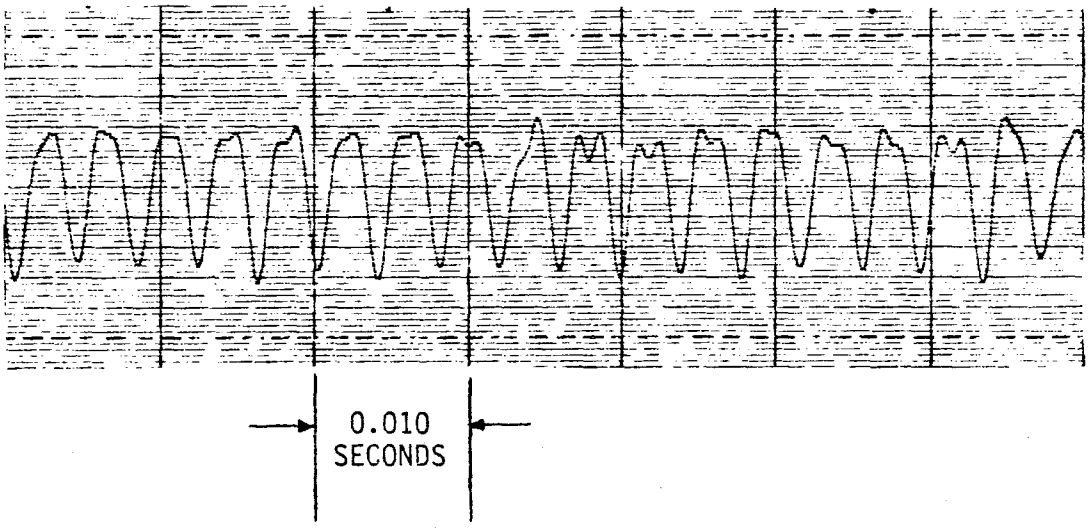

FIGURE 27. SSME LPFTP 82402 RESPONSE TIME HISTORY

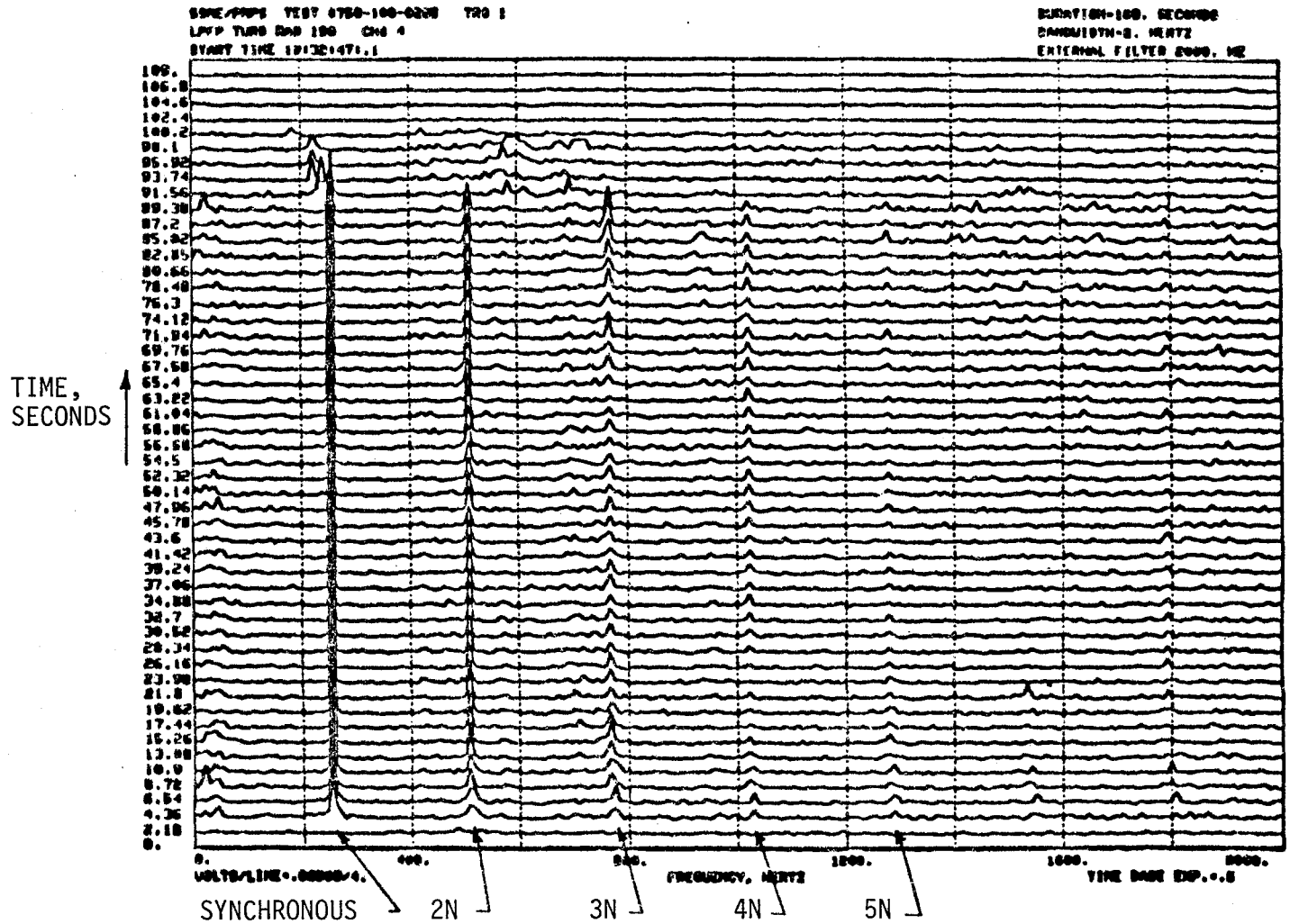

FIGURE 28. SSME LPFTP 82402 STEADY STATE RUBBING RESPONSE FREQUENCY VERSUS TIME

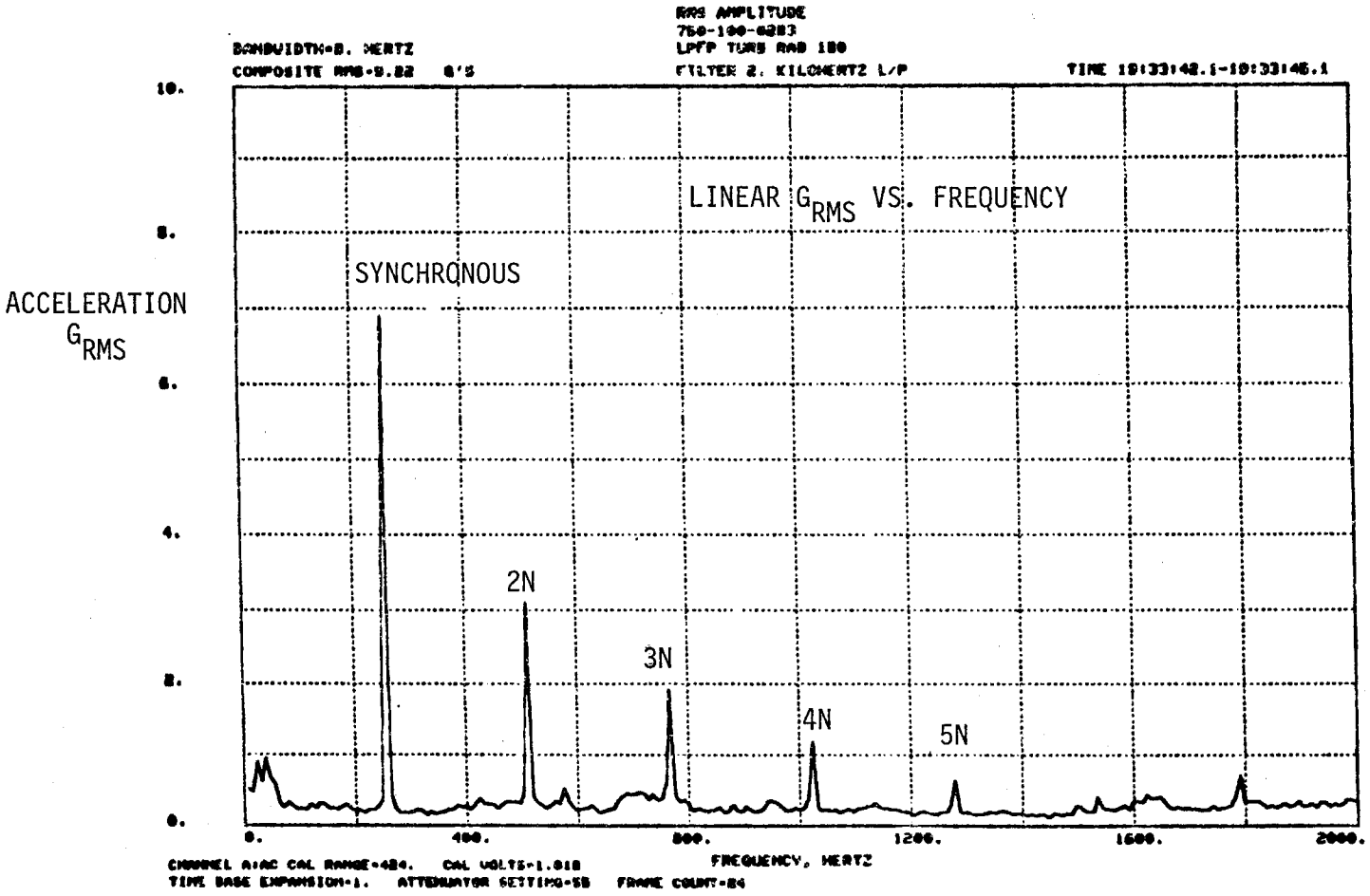

FIGURE 29. SSME LPFTP 82402 RUBBING RESPONSE SPECTRUM

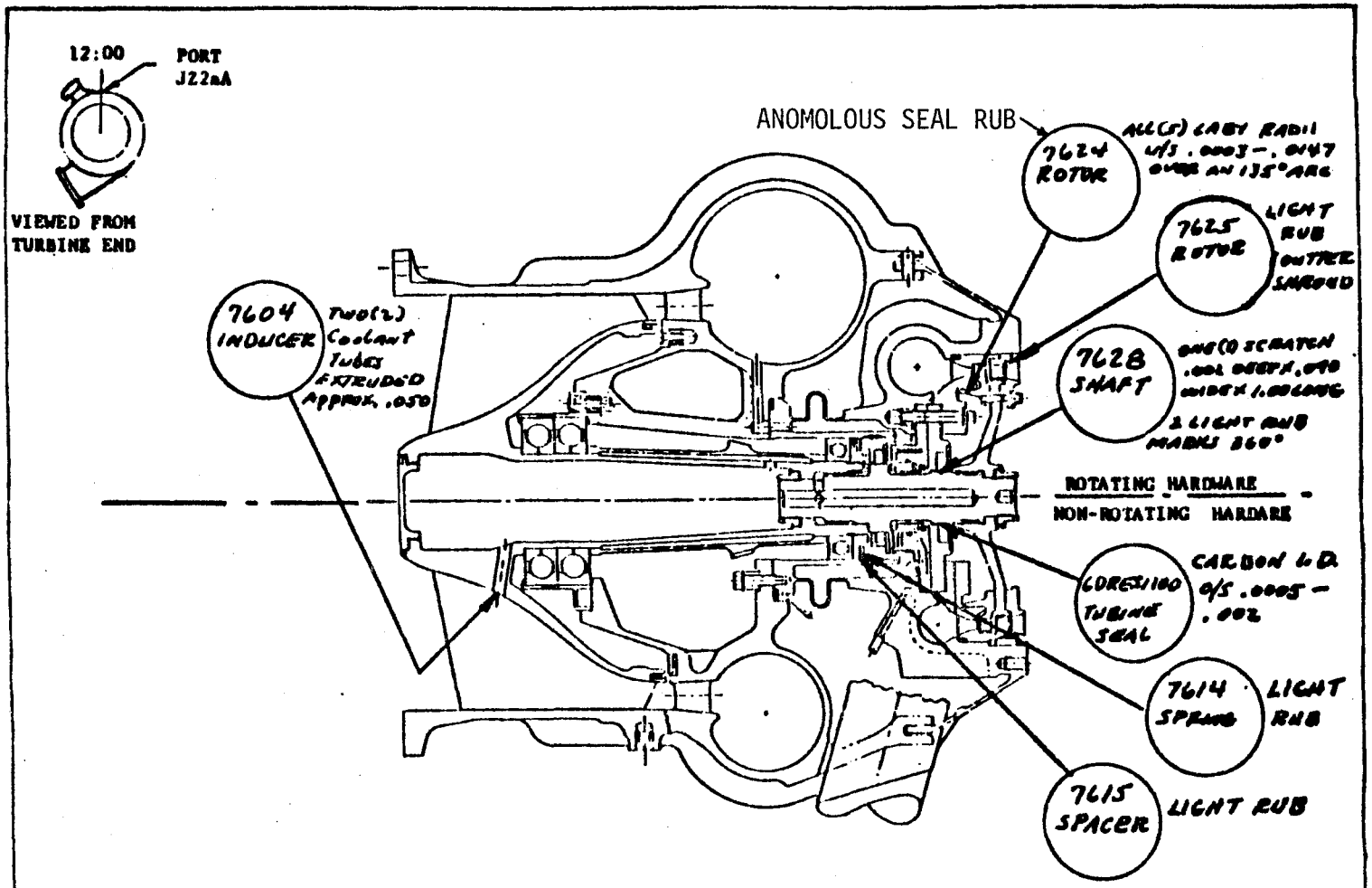

FIGURE 30. SSME LPFTP 82402 DISASSEMBLY REVIEW

HIGH PRESSURE FUEL TURBOPUMP

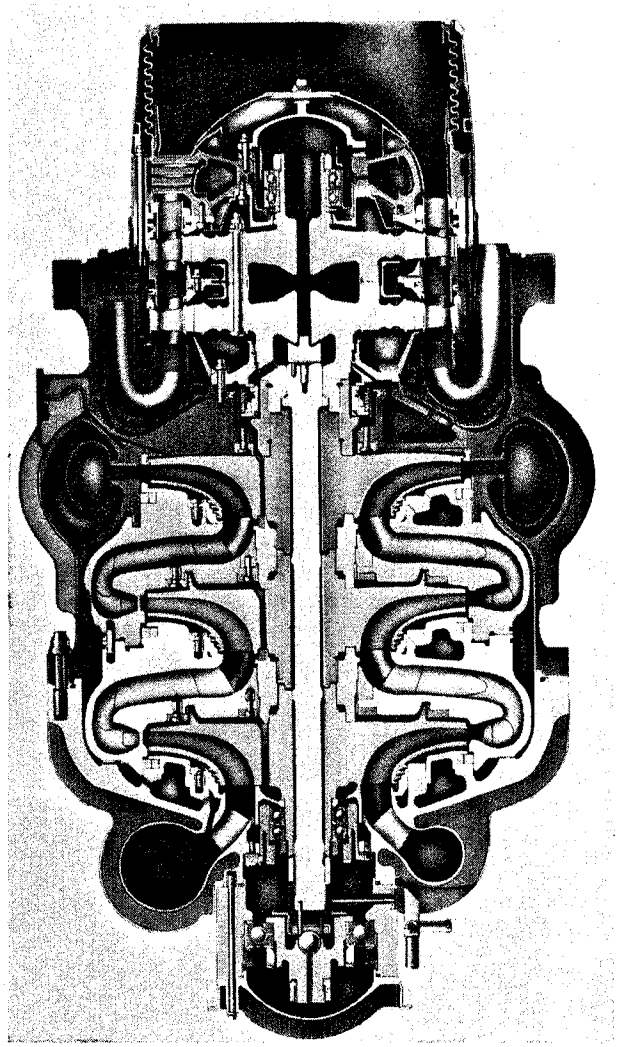

KEY PERFORMANCE PARAMETERS	RPL	FPL
PUMP INLET FLOWRATE LB/SEC	148.4	161.7
PUMP INLET PR PSIA	204.1	214.0
PUMP DISCH PR PSIA	6254.8	7036.8
PUMP EFFICIENCY	.758	.757
TURBINE FLOWRATE LB/SEC	147.5	164.0
TURBINE INLET TEMP R	1898.4	1989.2
TURBINE PRESSURE RATIO	1.522	1.558
TURBINE EFFICIENCY	.770	.780
TURBINE SPEED RPM	34931.	37076.
TURBINE HORSEPOWER	63288.	77142.

FIGURE 31. SPACE SHUTTLE MAIN ENGINE (SSME) HIGH PRESSURE FUEL TURBOPUMP (HPFTP)

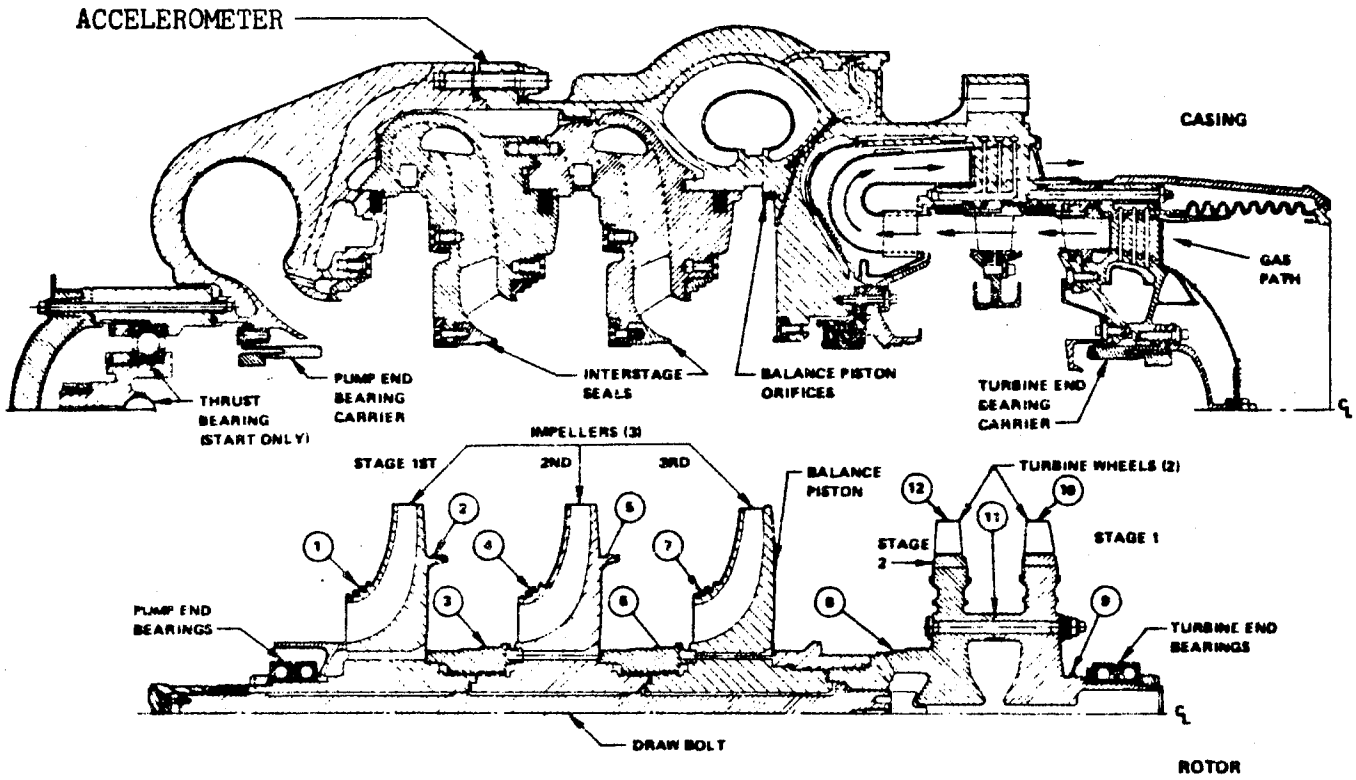

FIGURE 32. SSME HPFTP DESCRIPTION AND ACCELEROMETER LOCATION

TRACKING FILTER DATA
TEST: 902-147-8349
CONSTANT SPEED 35250 RPM

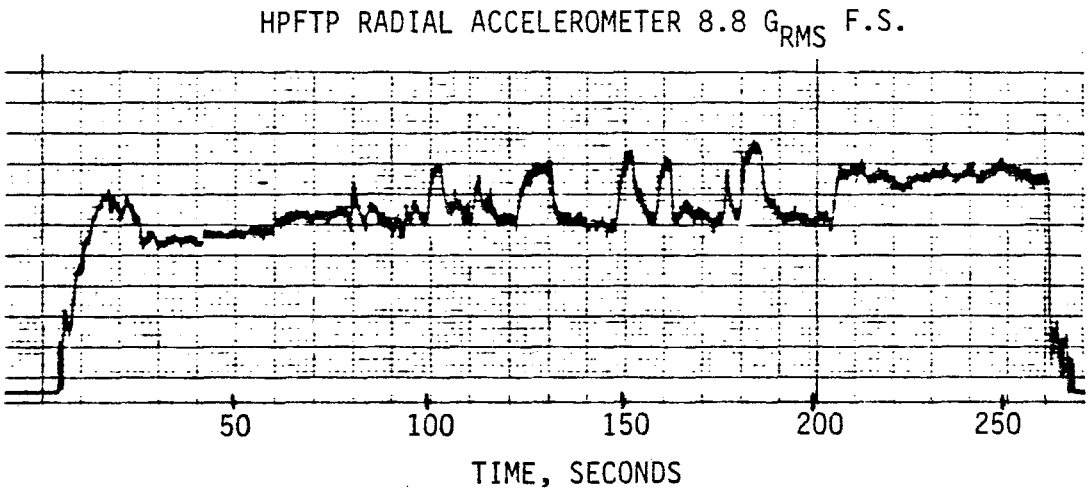

SPECTRAL DATA

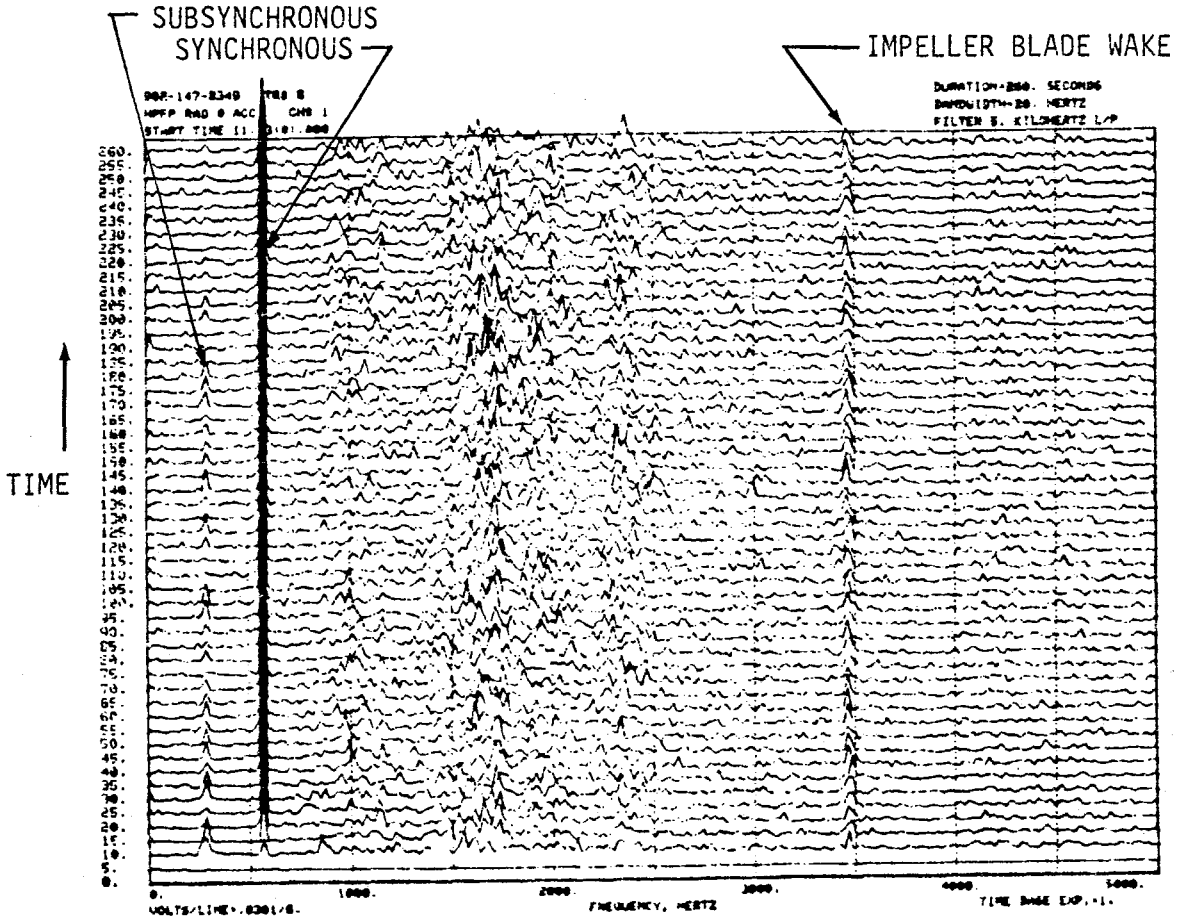

FIGURE 33. SSME HPFTP 2102R2 RUBBING DYNAMIC DATA

TRACKING FILTER DATA
TEST: 901-244-9163
CONSTANT SPEED 35500 RPM

HPFTP RADIAL ACCELEROMETER 11.2 G_{RMS} F.S.

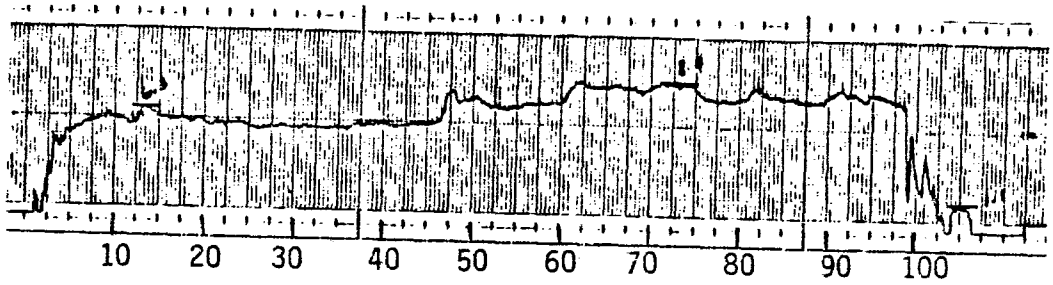

SPECTRUM DATA

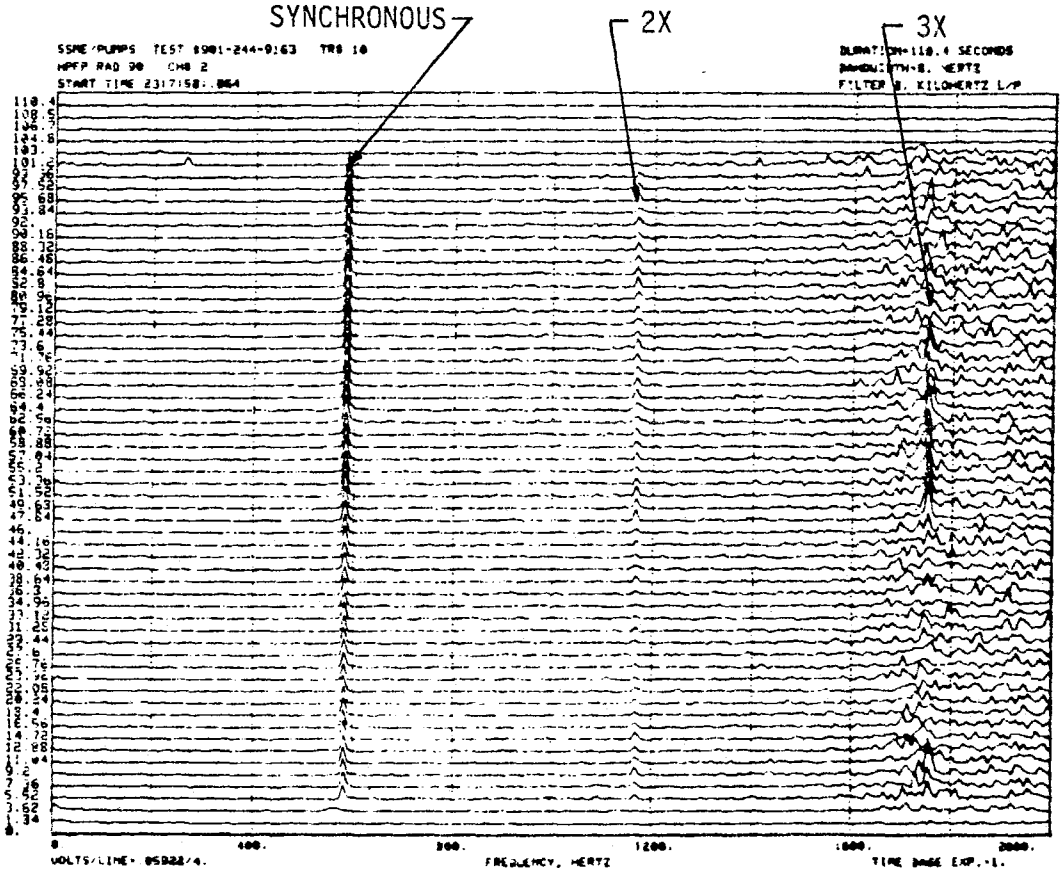

FIGURE 34. SSME HPFTP 0106 RUBBING DYNAMIC DATA

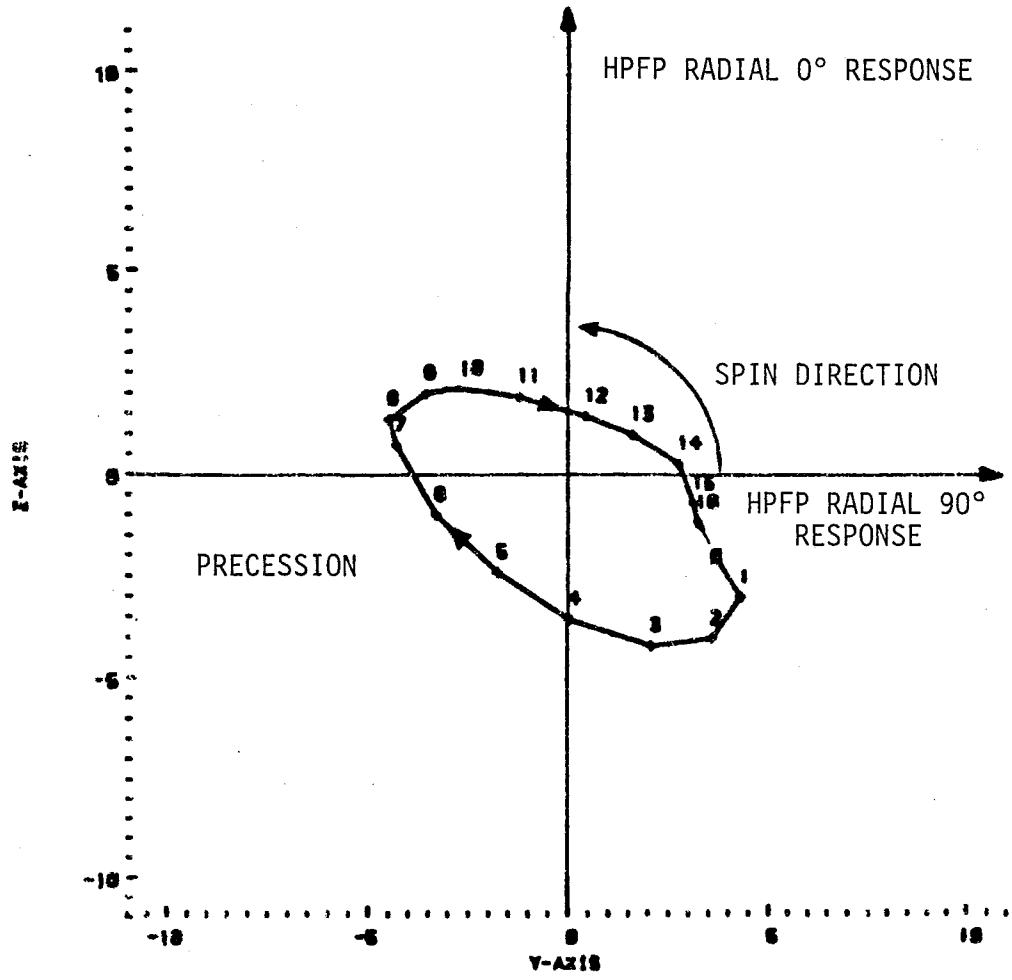

TEST 901-340 PUMP FLANGE ACCELEROMETER DATA AT 36300 RPM

FIGURE 35. SSME HPFTP 0210R4 BACKWARD SYNCHRONOUS PRECESSION

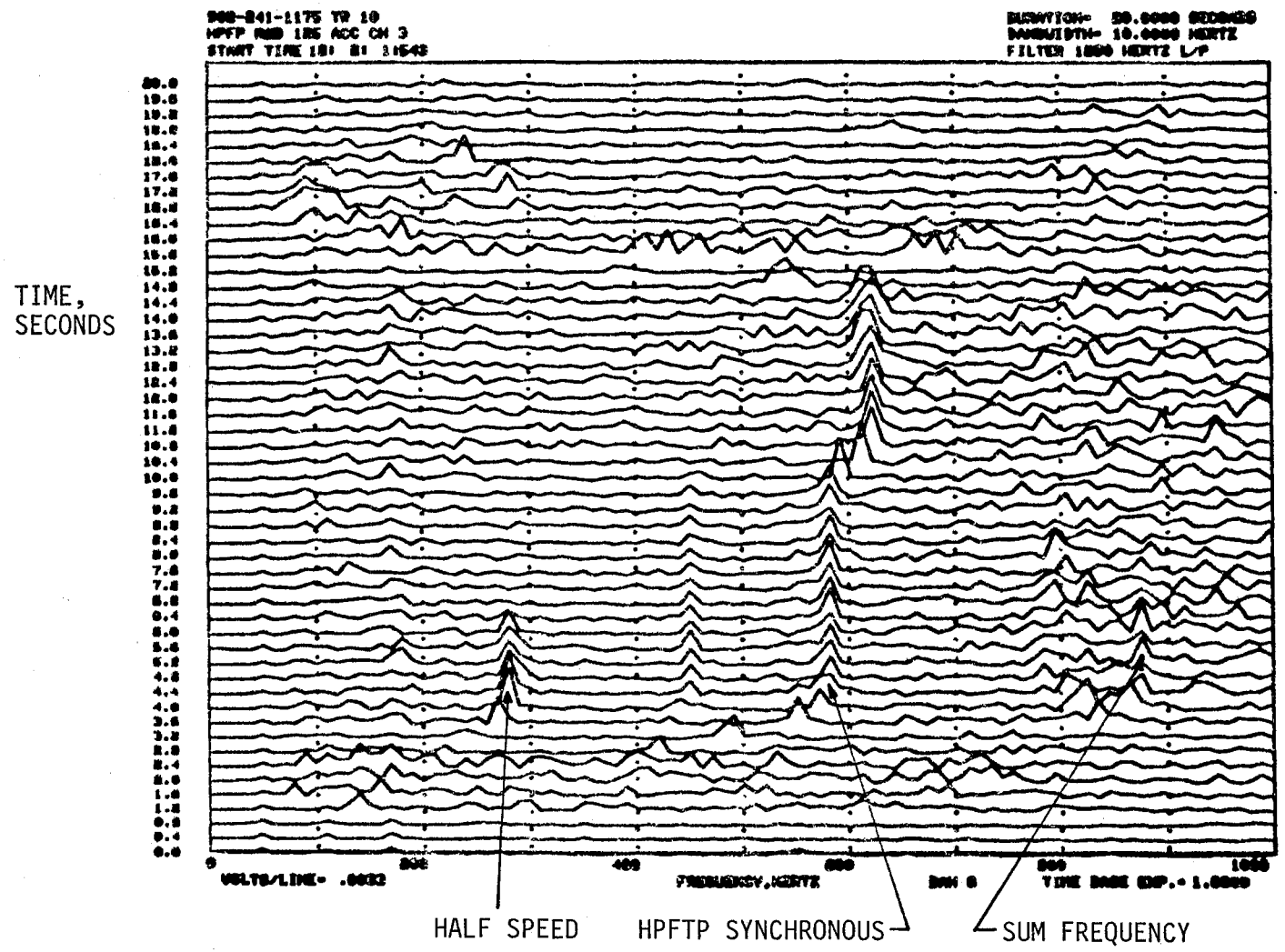

FIGURE 36. SSME HPFTP 9108 DEADBAND RESPONSE FREQUENCY VERSUS TIME

V. DISCUSSION

The predicted radial rotor rubbing response spectrum analysis bears a remarkable resemblance to the measured spectrum of both the SSME Low Pressure Fuel Turbopump (LPFTP) and the rotor kit. The rubbing response time history for the LPFTP in Figure 27 and the oscilloscope photograph for the rotor kit rubbing response in Figure 18 indicate the assumed shaft motion is a close approximation of the actual motion. The results demonstrate that the spectral analysis of the assumed shaft motion is qualitatively similar to the experimental data, with the second and third harmonics the major contributors in both cases. The excellent trend agreement between the spectral analyses gives credibility to the modelling technique. This is apparent by comparing the predicted results of Figure 36 for a 135° rotor rub arc with the measured LPFTP results of Figure 29 from a known 135° turbine seal rub arc test. For direct comparison, the results of the LPFTP and rotor kit testing are tabulated in Tables 1 and 2, respectively. Table 2 compares the results for approximately 140° to 150° of rotor contact arc based on the photograph of Figure 18. These experimental data comparisons agree with the predicted relative higher harmonic amplitudes trend. The significant trend correlation is the decreasing relative strength of the harmonics with increasing harmonic number.

In comparing the LPFTP spectral data, which is exact in frequency content, it should be noted that the measurement is located on the housing and isolated from the ideal location on the bearing support. In the literature, Ehrich (8) described how transmission

characteristics to housing mounted instrumentation, such as in the case of the LPFTP, can greatly amplify lower frequencies and attenuate higher frequencies. This effect, coupled with the nonlinear effect of the bearing clearance, is probably responsible for the discrepancies in the response amplitudes between the measured and predicted data of Table 1. Also, in comparing this data, the four times speed inducer blade wake vibration may mask the fourth harmonic amplitude data.

The rotor kit response comparison of Table 2 for a contact arc of approximately 140° to 150° shows a closer correlation of harmonic response amplitudes. This data was acquired with the benefit of displacement transducers sensing the shaft motion directly. The brass bearing small clearances are probably responsible for the slight amplitude differences.

Data interpretations based on the predicted response plotted in Figures 9 and 10, combined with the experimental data of Figure 23, can describe the rubbing progression from the initial stages to the eventual rotor instability as the gradually developing rotor rub arc increases. The response plotted in Figure 9 indicates that, as the harmonic amplitudes increase in the data, the threshold of a rotor instability approaches. Detecting this would indicate that more of the rotor circumference is in contact with the stator once per revolution. If the harmonic amplitudes decay with time, however, the rotor is probably wearing in and should operate without incident. For full contact rubbing, without a large frictional cross-coupling force, no harmonics are generated. Detection is indicated by backward synchronous precession on an orbit plot. The empirical data of Figure 23 shows the rubbing severity progression converges to the

commonly documented (Ehrich (6)) backward subsynchronous whirl instability near the rotor critical speed for a rotor in contact over the entire circumference at supercritical speed operation.

Many descriptions of rubbing imply that rubs are always instability drivers. This description of the phenomenon based on harmonic amplitude variations can be used to explain the potential for hazardous operation and why some rubbing rotors generally are stable if not in full contact with a sufficient frictional cross-coupling force.

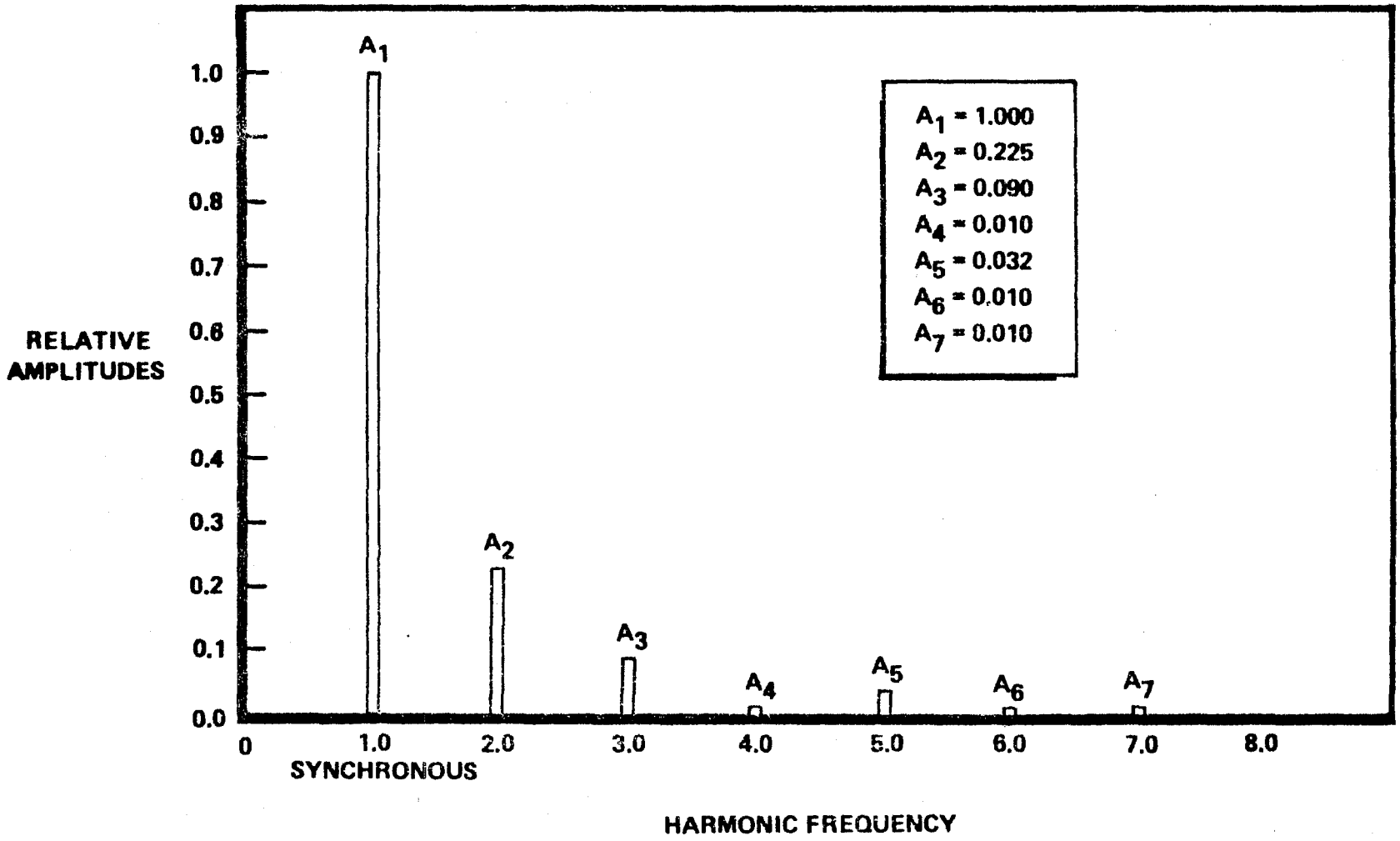

FIGURE 37. PREDICTED HARMONIC AMPLITUDE CONTENT FOR 135° ROTOR RUB ARC

TABLE 1.

a_n	LPFTP UNIT 82402 135° ROTOR RUB ARC HARMONIC AMPLITUDES NORMALIZED ACCELERATION ($\ddot{y}$)	VERSUS DISPLACEMENT* (y)	THEORETICAL PREDICTION 135° ROTOR RUB ARC HARMONIC AMPLITUDES DISPLACEMENT (y)
a_1	1.000	1.000	1.000
a_2	0.442	0.221	0.225
a_3	0.275	0.030	0.090
a_4	0.170**	0.010	0.010
a_5	0.086	0.003	0.032
a_6	0.057	0.001	0.010
a_7	0.072	0.001	0.010

* $y = \ddot{y}/\omega^2$

** Amplitude data may be distorted due to inducer blade wake generated vibration at four times speed.

TABLE 2.

EXPERIMENTAL RESULTS

Rotor kit response versus predicted response.

HARMONIC AMPLITUDE	ACTUAL RESPONSE FIGURE 20	NORMALIZED RESPONSE	*PREDICTED RESPONSE $\phi_1 = 70°$	*PREDICTED RESPONSE $\phi_1 = 75°$
a_1	0.0440	1.000	1.0	1.0
a_2	0.0100	0.227	0.246	0.288
a_3	0.0050	0.113	0.084	0.074
a_4	0.0020	0.045	0.015	0.034
a_5	0.0015	0.034	0.034	0.036

*Oscilloscope photograph indicates approximately 140° to 150° contact arc.

VI. RECOMMENDATIONS

It is recommended that upon review of the response data harmonic content, a rotor rub arc correlation of approximately 270° (ϕ_1 = 135°) be used as the separation point between benign and destructive contact. This separation point is selected because beyond this contact arc the fourth harmonic starts to increase sharply in its relative strength and leads a drastic increase in all the higher harmonics as shown in Figure 38. Observing these characteristics, or a backward synchronous precession in the experimental data should initiate a test termination, because it is probably only a matter of time until a catastrophic problem occurs. Monitoring the second and third harmonics only, test termination should be initiated when the second and third harmonics are approximately 75% and 50% of the synchronous amplitudes, respectively. Based on the data of Figure 36, if oscillations at 50% of shaft speed are observed; rubbing is not necessarily implied and the bearing clearances at speed should be evaluated.

It is also recommended that the data processing, evaluation and interpretation techniques presented using spectral analysis be implemented as part of a standard rubbing detection methodology. For each type of machine in test, an empirical data base should be maintained to establish reliable transfer functions relating the measured response to the actual rubbing location. The transfer function could also be obtained experimentally by performing a modal analysis of the housing, or analytically calculated with the use of finite element models of the rotor and housing. However, it is recognized that many projects do not have the luxury of these expensive analyses and the empirical method is

recommended. Once reliable specific amplitude limits have been established for a particular machine, a vibration cutoff system can be implemented. This system could be filtered around the synchronous frequency and/or the strong harmonic frequencies. If rubbing is detected, in most cases the problem can be alleviated by checking concentricities or improved balancing techniques. In situ balancing is recommended.

If the demonstration rotor kit testing were to be repeated, it is recommended that the rubbing time history be processed on oscillograph paper in addition to the oscilloscope photograph documentation. The shaft motion of both displacement transducers can then be saved for documentation and not limited by the single channel oscilloscope. It is also recommended that the bearing clearance be as tight as possible to avoid distortion of the response spectrum on any future rubbing test.

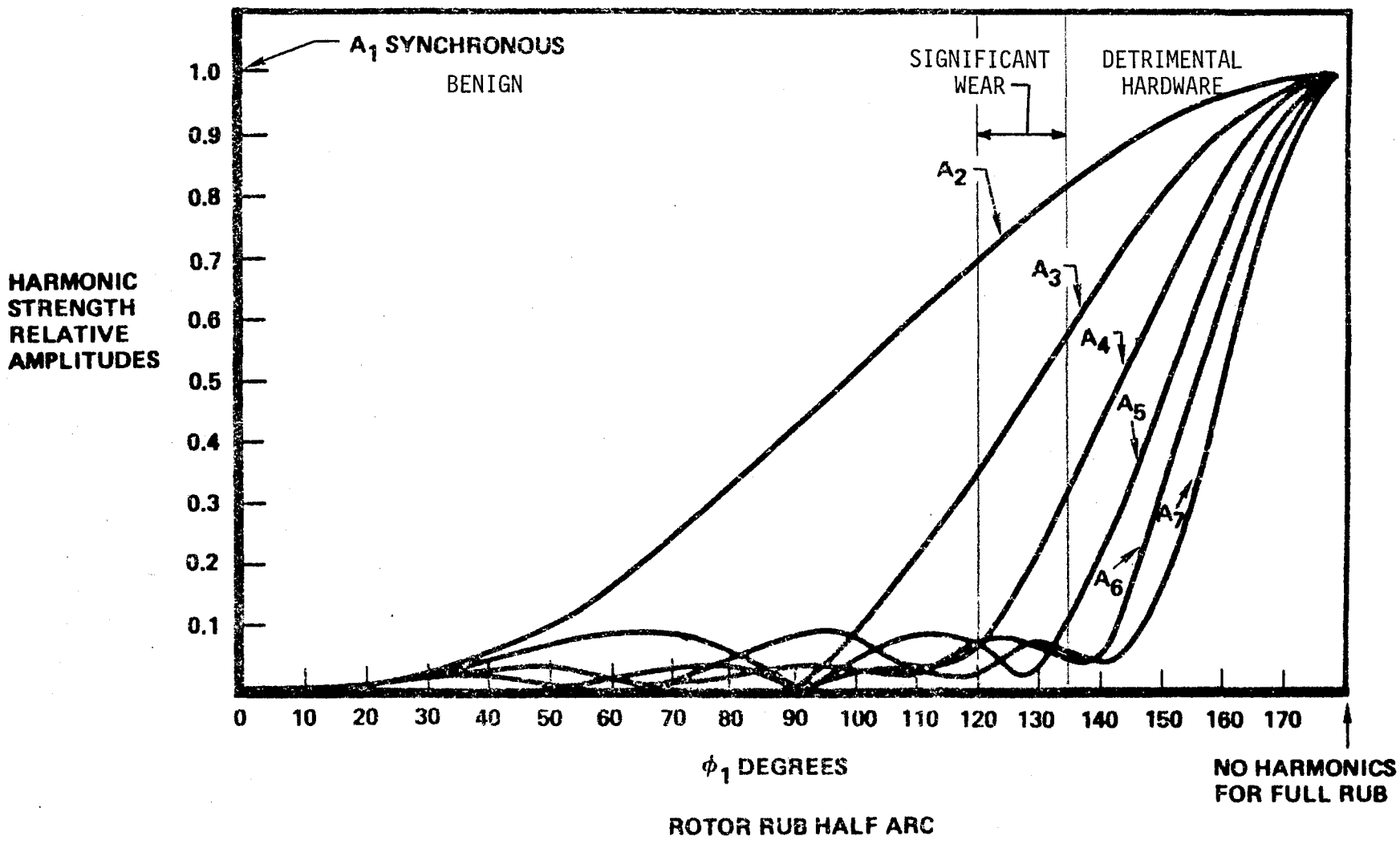

FIGURE 38. RUB SEVERITY FOR RELATIVE HARMONIC STRENGTH

VII. APPLICATION

Spectral analysis of rotoring machinery response is nothing new, ball bearing investigators have been using it in defect detection for a number of years. In expanding this analysis for rubbing detection, some general procedures should be adopted. This includes identifying the source of typical frequencies and determining the normal amplitude ranges. The frequencies and amplitudes should be related to operating speed and hardware conditions. In doing so, a spectrum analysis monitoring system can be established to investigate the rotor rubbing response during steady state operation. Applying the techniques presented herein, a harmonic frequency amplitude growth can be related to a rubbing severity increase. A reduction in harmonic frequency amplitudes can be related to a decrease in rubbing. In addition, the differentiating techniques between benign and destructive contact, and between bearing deadband response can be employed. A development program to establish a reliable data base and trend relationship for a particular machine should provide guidance in scheduling of necessary machine maintenance.

As a case history, Patton (15) has used the methods presented to accurately determine turbine area rubbing in MK48-0 turbopump testing, This stopped additional testing and prevented further hardware damage. It was a crucial decision since this machine pumps liquid oxygen, making the rubbing surface an explosion source. Disassembly revealed heavy turbine floating ring seal rubbing damage and turbine tip seal rubbing.

This information is provided for the rotordynamics engineer as

an early detection method of rotor rubbing. Where the rub progression is from test to test with data evaluation between tests, early detection could minimize the wearing hardware damage and reduce replacement costs and inactive time. It should be pointed out that this simplified approach is very basic and needs empirical data support to be effective. The method can detect rubbing in general and possibly the predominate direction, it cannot locate a specific location on the rotor as the rubbing point. Therefore, it is impossible to predict the exact rubbing seal, for example, without transfer function data correlation.

It should be noted that harmonics greater than the third for a reasonable contact arc are such a small percentage of the synchronous amplitude that, in practicality, these voltages in the analog/digital system may be too low to detect and masked by the instrumentation noise floor. If unexplained harmonics greater than the third are observed it is suggested to inspect the hardware because a variety of nonlinear problems may be occurring.

VIII. CONCLUSIONS

Rotor response has been described due to radial rubbing as a function of the rotor contact circumference based on a combination of analytical and experimental results. The response was calculated in terms of a Fourier series expansion of a predicted rub-induced shaft motion. Relative response amplitudes of the generated harmonic frequency spectrum were presented as the identifying rub characteristic, particularly two and three times speed. Experimental data from both industry examples and a controlled laboratory rubbing test on a demonstration rotor kit were provided for comparison with the analytical prediction.

Although the examples discussed are limited to turbomachinery, this analysis technique is general enough to apply to all rotating machinery. No stipulation is made with respect to the operational speed relationship to the critical speed. In the examples, the LPFTP operates below its critical speed and the rotor kit operates above its critical speed. There are other variables which can effect the total rotor response, such as bearing clearances, yet this simplified approach to analyzing rubbing tends to agree with experimental data well enough to develop a reliable detection methodology.

Spectral analysis of rotor rubbing time histories has proven to be a valuable tool in defining and detecting distinct harmonic response characteristics. The harmonic data trends discussed should be monitored as an identifying rub characteristic. In general, the following is concluded as advancing the state of the art in rubbing detection;

1) The second and third harmonics of the synchronous speed frequency are produced during a rubbing condition with the second greater than the third.
2) Benign rubbing can be expected for a rotor contact arc of less than 270°, or the second and third harmonic amplitudes less than 75% and 50% of the synchronous response, respectively.
3) Full contact rubbing with a significant frictional cross-coupling force leads to a rotor instability.
4) Monitoring of only synchronous vibration can be misleading for rubbing evaluation. The entire spectrum requires evaluation.
5) Bearing deadband response produces subsynchronous oscillations at 50% of shaft speed and differs from the rubbing nonlinearity response.

The significance of these results is that dynamic response characteristics can now be related to the degree of rotor rubbing. Essentially, the harmonic amplitudes increase as the rub progresses to contact more of the rotor circumference leading to excessive wear, a rotor instability or shaft seizure. The analyst should evaluate test data by tracking the harmonic amplitudes and monitor performance. This allows for scheduling maintenance before the condition becomes too severe.

IX. FURTHER EVALUATIONS

More work is needed, both analytically and experimentally, in determining the response spectrum of rotating machinery which may have significant bearing clearances during a rubbing condition. Such a situation may be present on a test of a HPFTP, as shown in Figure 39. This spectrum indicates the generation of subsynchronous, synchronous, supersynchronous, and sums and difference frequencies. Determining a proper interpretation of this data is rather difficult to achieve based on today's state of the art evaluations. An interpretation, based on the results presented herein, could be that the rotor starts out with synchronous and bearing deadband motion, a speed increase occurs at approximately 250 seconds and the subsynchronous oscillations shift to the rotor first critical speed frequency. At this time, sum and difference frequencies occur indicating that an additional non-linearity, such as rubbing, has occurred. Without an in depth analysis, this correlation interpretation can only be considered feasible conjecture of course. However, nothing was found in the hardware inspection to dispute the scenario.

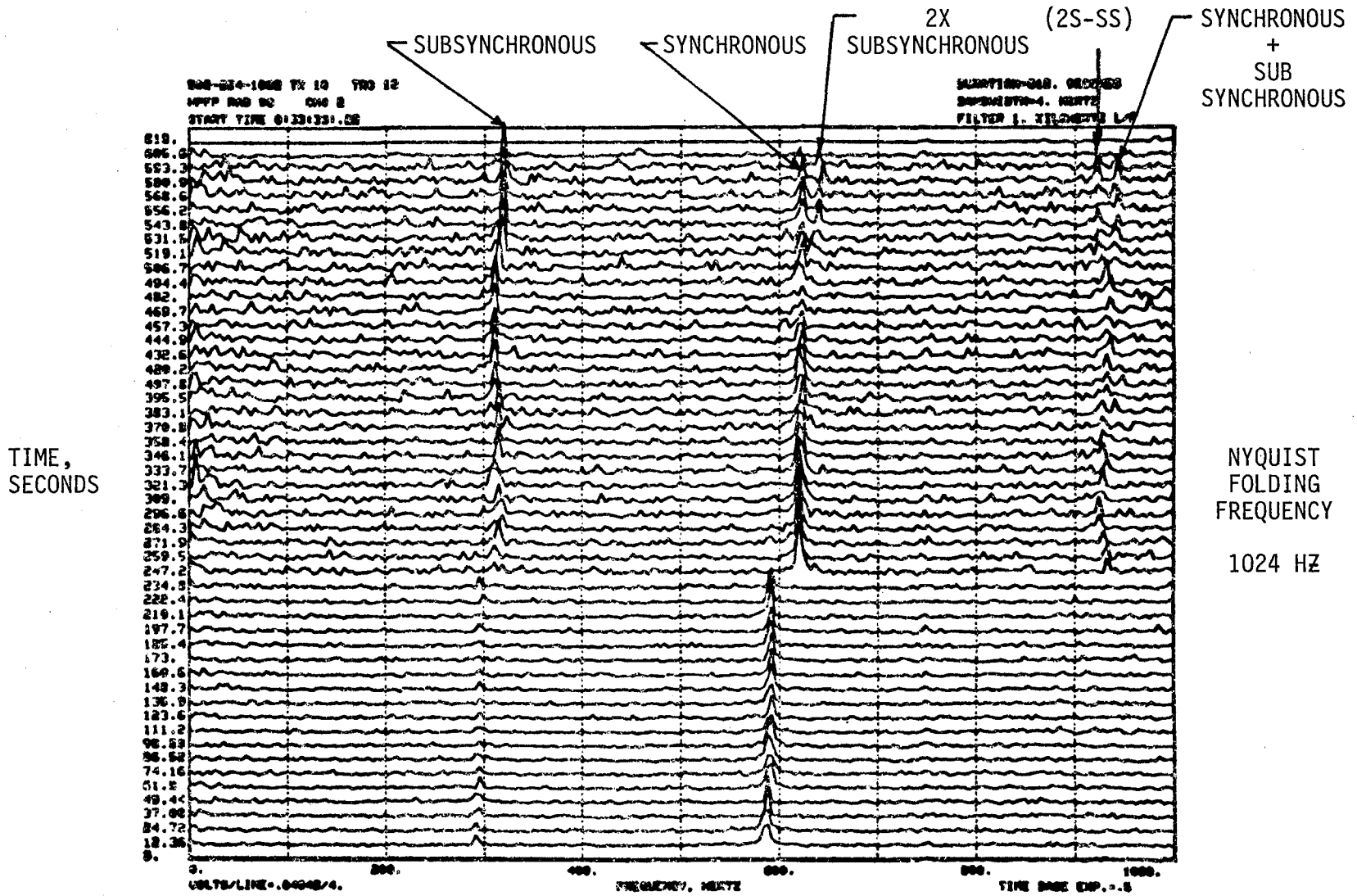

FIGURE 39. SSME HPFTP 0208R1 RESPONSE FREQUENCY VERSUS TIME

X. ACKNOWLEDGEMENTS

The author is grateful to Rocketdyne Structural Dynamics for the use of the rotor kit and the Rocketdyne Analog Room for the use of the RTDA. Special thanks to Jim Miller, the Real Time Data Analyzer operator, and Jim Fenwick, who assisted in conducting the experiments.

The Space Shuttle Main Engine Turbopumps used as examples were developed by Rocketdyne for NASA Marshall Space Flight Center, Huntsville, Alabama, under contract NAS8-27980.

XI. REFERENCES

1. Black, H. F. and D. N. Jenssen, "Effects of High Pressure Ring Seals on Pump Rotor Vibrations," ASME Paper 71-WA/FE-38.
2. Alford, J. S., "Protecting Turbomachinery from Self-Excited Rotor Whirl," Journal of Engineering for Power, October 1965.
3. Den Hartog, J. P., Mechanical Vibrations, Fourth Edition, McGraw-Hill, 1956.
4. Kascak, A. F., "The Response of Turbine Engine Rotors to Interference Rubs," NASA TM 81581, AVRADCOM TR80-C-14, June 1980.
5. Ek, M. C., "Solving Subsynchronous Whirl in the High-Pressure Hydrogen Turbomachinery of the SSME," AIAA 78-1002R, May-June 1980, Page 208.
6. Ehrich, F. F., "The Dynamic Stability of Rotor/Stator Radial Rubs in Rotating Machinery," Journal of Engineering for Industry, ASME Trans, Nov. 1969, pgs. 1025-1028.
7. Ehrich, F. F., "Sub-Harmonic Vibration of Rotors in Bearing Clearances," ASME Paper 66-MD-1, Design Engineering Conference, Chicago, Ill., May 9-12, 1966.
8. Ehrich, F. F., "Sum and Difference Frequencies in Vibration of High Speed Rotating Machinery," Journal of Engineering for Industry, ASME Trans., February 1972, pgs. 181-184.
9. Bently Engineering Staff, Operating Manual for Rotor Kit, March, 1979.
10. Bently, D. E., "Forced Subrotative Speed Dynamic Action of Rotating Machinery," ASME Paper 74-PET-16, Petroleum Mechanical Engineering Conference, Dallas, Texas, Sept. 15-18, 1974.

11. Childs, D. W., "Rub-Induced Parametric Excitation in Rotors," ASME Paper 78-WA/DE-14, The American Society of Mechanical Engineers, San Francisco, Calif., December 10-15, 1978.

12. Taylor, H. D., "Rubbing Shafts Above and Below the Resonance Speed (Critical Speed)," General Electric Company, Schenectady, N.Y., R-16709, April 29, 1924.

13. Beatty, R. F., "CRITSP and ROTPLT Critical Speed Calculation and Plotting Program Users Guide," Rocketdyne Division of Rockwell International Internal Letter, 0113-3237, dated October 22, 1980.

14. Tepfer, W. E., "Disassembly Review - LPFTP Unit 82402, "Rocketdyne Division of Rockwell International Internal Letter 0170TM-732, SSME 80-2659, dated December 22, 1980.

15. Patton, M. P., "MK48-0 Dynamic Data Analyses," Rocketdyne Division of Rockwell International Internal Letter 1127-3089, dated June 18, 1981.

XII. APPENDIX

A. FOURIER SERIES EXPANSION

THE FOURIER SERIES ANALYSIS OF THE ASSUMED SHAFT MOTION

ASSUMPTIONS AND DESCRIPTION OF METHOD

Let it be assumed that partial rubbing is by definition light rubbing and that the rotor comes in contact with the stator once per revolution. The resulting shaft motion is shown in Figure 8. One complete revolution of the rotor represents one complete cycle. The resulting wave form, varying in amplitude from A to -1.0, is defined as:

$$f(\phi) = A \qquad \text{for } -\phi_1 \leq \phi \leq \phi_1$$

$$f(\phi) = \cos\phi \qquad \text{for } \phi_1 \leq \phi \leq -\phi_1$$

Where A is the truncated amplitude of the rotor and ϕ is angular position.

A Fourier series of the form below describes the complete cyclic response.

$$(F\phi) = \frac{a_o}{2} + \sum_{n=1}^{\infty} (a_n \cos n\omega t + b_n \sin n\omega t)$$

where: $a_o/2$ represents the average static value of $F(\phi)$ and ωt is the frequency sweep.

The coefficients of the series terms are given by

$$a_n = \frac{1}{L} \int_{-L}^{L} f(\phi) \cos n\phi \, d\phi, \quad n = 0,1,2,3.....$$

$$b_n = \frac{1}{L} \int_{-L}^{L} f(\phi) \sin n\phi \, d\phi, \quad n = 1,2,3.....$$

$f(\phi)$ is an even function (ie $f(-\phi) = f(\phi)$) so therefore the Fourier series reduces to:

$$\frac{a_o}{2} + \sum_{n=1}^{\infty} a_n \cos n\omega t$$

a_n = amplitude of harmonic
ω = frequency

That is, $b_n = 0$. For this case, a simplier formula for a_n is

$$a_n = \frac{2}{L} \int_0^L f(\phi) \cos n\phi d\phi$$

Where: $L = \pi$

ϕ_1 = half contact rotor arc

$A = \cos\phi_1$

$$a_o = \frac{2}{\pi}\left[\int_o^{\phi_1} A d\phi + \int_{\phi_1}^{\pi} \cos\phi d\phi\right] = \frac{2}{\pi}\left[A\phi_1 + \sin\pi - \sin\phi_1\right]$$

$$a_o = \frac{2}{\pi}\left[\phi_1\cos\phi_1 - \sin\phi_1\right]$$

$$\frac{a_o}{2} = \frac{1}{\pi}\left[\phi_1\cos\phi_1 - \sin\phi_1\right] \Bigg\} \text{ D.C. or Static Value}$$

$$a_n = \frac{2}{\pi}\left[\int_o^{\phi_1} A \cos n\phi d\phi + \int_{\phi_1}^{\pi} \cos\phi\cos n\phi d\phi\right]$$

$$n\neq 1 \quad a_n = \frac{2}{\pi}\left[\frac{A}{n}\sin n\phi\Big|_o^{\phi_1} + \left[\frac{\sin(1-n)\phi}{2(1-n)} + \frac{\sin(1+n)\phi}{2(1+n)}\right]\Bigg|_{\phi_1}^{\pi}\right]$$

$$\int(\cos mx)\ (\cos nx)dx = \frac{\sin(m-n)x}{2(m-n)} + \frac{\sin(m+n)x}{2(m+n)}, \quad (m^2 \neq n^2)$$

Harmonics
$n = 2,3\ldots$

$$a_n = \frac{2}{\pi}\left[\frac{\cos\phi_1}{n}\sin n\phi_1 - \left[\frac{\sin(1-n)\phi_1}{2(1-n)} + \frac{\sin(1+n)\phi_1}{2(1+n)}\right]\right]$$

$$a_n = \frac{2}{\pi}\left[\frac{\cos\phi_1 \sin n\phi_1}{n} - \frac{\sin(n-1)\phi_1}{2(n-1)} - \frac{\sin(n+1)\phi_1}{2(n+1)}\right]$$

$$a_n = \frac{2}{\pi}\left[\frac{\cos\phi_1 \sin n\phi_1}{n} - \left[\frac{\sin n\phi_1 \cos\phi_1 - \cos n\phi_1 \sin\phi_1}{2(n-1)}\right] - \left[\frac{\sin n\phi_1 \cos\phi_1 + \cos n\phi_1 \sin\phi_1}{2(n+1)}\right]\right]$$

$$a_n = \frac{2}{\pi}\left[\sin n\phi_1 \cos\phi_1\left[\frac{1}{n} - \frac{1}{2(n-1)} - \frac{1}{2(n+1)}\right] + \cos n\phi_1 \sin\phi_1 \left[\frac{1}{2(n-1)} - \frac{1}{2(n+1)}\right]\right]$$

$$a_n = \frac{2}{\pi}\left[\frac{-1}{n(n^2-1)}\ \sin n\phi_1\ \cos\phi_1 + \frac{1}{(n^2-1)}\ \cos n\phi_1\ \sin\phi_1\right];\ n = 2,3.....$$

a_n = amplitude of harmonics

$$a_n = \frac{2}{\pi}\left[\frac{\cos n\phi_1\ \sin\phi_1}{(n^2-1)} - \frac{\sin n\phi_1\ \cos\phi_1}{n(n^2-1)}\right] \quad \text{where } n = 2,3,4.....$$

Now solve for synchronous amplitude when n = 1

n=1 $$a_1 = \frac{2}{\pi}\left[\int_o^{\phi_1} A\cos\phi d\phi + \int_{\phi_1}^{\pi} \cos^2\phi d\phi\right]$$

$$\int\cos^2 x dx = [1/2]x + 1/4[\sin 2x]$$

$$a_1 = \frac{2}{\pi}\left[A(\sin\phi)\ \Big|_o^{\phi_1} + \left(\frac{\phi}{2} + \frac{\sin 2\phi}{4}\right)\ \Big|_{\phi_1}^{\pi}\right]$$

$$a_1 = \frac{2}{\pi}\left[A\ \sin\phi_1 + \left(\frac{\pi}{2} + \frac{\sin 2\pi}{4}\right) - \left(\frac{\phi_1}{2} + \frac{\sin 2\phi_1}{4}\right)\right]$$

$$A = \cos\phi_1$$

$$a_1 = \frac{2}{\pi}\left[\cos\phi_1\ \sin\phi_1 + \frac{\pi}{2} - \frac{\phi_1}{2} - \frac{\sin 2\phi_1}{4}\right]$$

$$a_1 = \frac{2}{\pi}\ \cos\phi_1 \sin\phi_1 + 1 - \frac{\phi_1}{\pi} - \frac{\sin 2\phi_1}{2\pi}$$

$$a_1 = 1 - \frac{\phi_1}{\pi} + \frac{2}{\pi}\sin\phi_1\ \cos\phi_1 - \frac{1}{\pi}\ \sin\phi_1\ \cos\phi_1$$

$$a_1 = 1 - \frac{\phi_1}{\pi} + \frac{1}{\pi}\sin\phi_1\ \cos\phi_1$$

$$a_1 = 1 - \frac{\phi_1}{\pi} + \frac{\sin 2\phi_1}{2\pi}\Bigg\} \text{ synchronous amplitude}$$

Summarizing: $\frac{a_o}{2} + \sum_{n=1}^{\infty} a_n \cos n\omega t$ = rotor response

(D.C.) Static Amplitude = $\frac{a_o}{2} = \frac{1}{\pi}\left[\phi_1\ \cos\phi_1 - \sin\phi_1\right]$

(ω) Synchronous Amplitude = $a_1 = 1 - \frac{\phi_1}{\pi} + \frac{\sin 2\phi_1}{2\pi}$

$$(n\omega) \qquad \text{Harmonic Amplitudes} = a_n = \frac{2}{\pi}\left[\frac{\cos n\phi_1 \sin\phi_1}{(n^2-1)} - \frac{\sin n\phi_1 \cos\phi_1}{n(n^2-1)}\right]$$

As ϕ_1 converges to 0°, only the synchronous amplitude equal to 1.0 should remain and this checks. As ϕ_1 converges to 180°, or π, the location becomes a bearing, always in contact at a constant value and generates no harmonics. Assume steady state and a typical rotor rub arc = 180°, then ϕ_1 = 90°, or $\pi/2$

$$\frac{a_o}{2} = -\frac{1}{\pi}$$

$$a_1 = 0.500$$

$$a_2 = 0.2122$$

$$a_3 = 0.0$$

$$a_4 = 0.0424$$

$$a_5 = 0.0$$

$$a_6 = 0.01818$$

$$a_7^{*} = 0.0$$

* Higher harmonic could not be seen in data.

So for $\phi_1 = \frac{\pi}{2}$ only even harmonics are produced. For rotor rub arcs $\neq \frac{\pi}{2}$ all harmonics are produced. It is necessary to plot harmonic amplitude vs. rub arc to determine the response spectrum for all ϕ_1. Of note here is that for a normalized synchronous amplitude of 1.0 the second harmonic is 42% of synchronous. This amplitude should be easily seen in the data.

XII. APPENDIX

B. DATA PROCESSING TECHNIQUES

The following is a description of the data processing techniques used in rotating machinery analysis. Most of the processing employs a Real Time Data Analyzer (RTDA). This machine is capable of calculating the response spectrum using time series analysis. Digital computer software utilizing a Fast Fourier Transform (FFT) analysis is used to generate the output. Pertanent to understanding the output from this machine is a basic knowledge of how the digital process operates. Over the frequency range of interest, the analysis is capable of certain resolutions which subdivides the whole frequency range into equal component frequency bands. The resolution then determines the analysis bandwidth. The inverse of the bandwidth (Hz) equals the time required to acquire a block of data, called a frame. Between acquiring frames of data is a certain amount of machine processing time. Frames of data are acquired until the whole time slice of interest is covered. The frequency range of interest is low pass filtered and significant data slightly above the Nyquist Folding Frequency can be displayed as the mirror image about this frequency as shown in Figure 38. The specific computer programs used in this thesis are;

1) Amplitude Spectrum: plots the root mean square (RMS) amplitude versus frequency over a steady state time slice. For rotating machinery analysis, this processing is capable of plotting the synchronous and harmonic amplitudes for a particular time slice.
2) Isoplot: a series of single frame amplitude spectra obtained at selected equally spaced time intervals displayed in a single plot as frequency versus time. For rotating machinery analysis,

frequency variations of synchronous and harmonic amplitudes for changes in speed can be plotted versus time.

An analog system was used to process the tracking filter data.

3) Tracking Filter: In this analysis, two signals are acquired simultaneously. One is of time varying frequency on a reference channel. This is the frequency which is tracked. The narrow band filtered RMS amplitude of the second signal about the frequency of the first signal is computed. In rotating machinery analysis, this processing can be used to plot synchronous amplitudes versus speed or time.